VU VRIJE UNIVERSITEIT AMSTERDAM

VU Research Portal

Sedimentary dynamics and high-frequency sequence stratigraphy of the southwestern slope of Great Bahama Bank

Wunsch, Marco; Betzler, Christian; Eberli, Gregor P.; Lindhorst, Sebastian; Lüdmann, Thomas; Reijmer, John J.G.

published in
Sedimentary Geology
2018

DOI (link to publisher)
10.1016/j.sedgeo.2017.10.013

document version
Publisher's PDF, also known as Version of record

document license
Article 25fa Dutch Copyright Act

Link to publication in VU Research Portal

citation for published version (APA)
Wunsch, M., Betzler, C., Eberli, G. P., Lindhorst, S., Lüdmann, T., & Reijmer, J. J. G. (2018). Sedimentary dynamics and high-frequency sequence stratigraphy of the southwestern slope of Great Bahama Bank. *Sedimentary Geology*, *363*, 96-117. https://doi.org/10.1016/j.sedgeo.2017.10.013

General rights
Copyright and moral rights for the publications made accessible in the public portal are retained by the authors and/or other copyright owners and it is a condition of accessing publications that users recognise and abide by the legal requirements associated with these rights.

- Users may download and print one copy of any publication from the public portal for the purpose of private study or research.
- You may not further distribute the material or use it for any profit-making activity or commercial gain
- You may freely distribute the URL identifying the publication in the public portal ?

Take down policy
If you believe that this document breaches copyright please contact us providing details, and we will remove access to the work immediately and investigate your claim.

E-mail address:
vuresearchportal.ub@vu.nl

Download date: 05. May. 2023

Sedimentary Geology 363 (2018) 96–117

Contents lists available at ScienceDirect

Sedimentary Geology

journal homepage: www.elsevier.com/locate/sedgeo

Sedimentary dynamics and high-frequency sequence stratigraphy of the southwestern slope of Great Bahama Bank

Marco Wunsch [a,*], Christian Betzler [a], Gregor P. Eberli [b], Sebastian Lindhorst [a], Thomas Lüdmann [a], John J.G. Reijmer [c]

[a] Institut für Geologie, Universität Hamburg, Bundesstr. 55, 20146 Hamburg, Germany
[b] Center for Carbonate Research, University of Miami, 4600 Rickenbacker Causeway, Miami, FL 33149, USA
[c] College of Petroleum Engineering and Geosciences, King Fahd University of Petroleum & Minerals, KFUPM Box 2263, Dhahran 31261, Saudi Arabia

ARTICLE INFO

Article history:
Received 4 July 2017
Received in revised form 26 October 2017
Accepted 27 October 2017
Available online 3 November 2017

Editor: Dr. B. Jones

Keywords:
Bahamas
Carbonate slopes
Contour currents
Slope morphology
Seismic stratigraphy
Facies modeling

ABSTRACT

New geophysical data from the leeward slope of Great Bahama Bank show how contour currents shape the slope and induce re-sedimentation processes. Along slope segments with high current control, drift migration and current winnowing at the toe of slope form a deep moat. Here, the slope progradation is inhibited by large channel incisions and the accumulation of large mass transport complexes, triggered by current winnowing. In areas where the slope is bathed by weaker currents, the accumulation of mass transport complexes and channel incision is rather controlled by the position of the sea level. Large slope failures were triggered during the Mid-Pleistocene transition and Mid-Brunhes event, both periods characterized by changes in the cyclicity or the amplitude of sea-level fluctuations. Within the seismic stratigraphic framework of third order sequences, four sequences of higher order were identified in the succession of the upper Pleistocene. These higher order sequences also show clear differences in function of the slope exposure to contour currents. Two stochastic models emphasize the role of the contour currents and slope morphology in the facies distribution in the upper Pleistocene sequences. In areas of high current influence the interplay of erosional and depositional processes form a complex facies pattern with downslope and along strike facies alterations. In zones with lower current influence, major facies alternations occur predominately in downslope direction, and a layer-cake pattern characterizes the along strike direction. Therefore, this study highlights that contour currents are an underestimated driver for the sediment distribution and architecture of carbonate slopes.

© 2017 Elsevier B.V. All rights reserved.

1. Introduction

The slopes of carbonate platforms provide key information on the adjoined carbonate factory and the factors controlling the platform evolution (Eberli and Ginsburg, 1987; Tinker, 1998; Betzler et al., 1999; Verwer et al., 2009). The broad grain-size spectrum and the diversity of the re-sedimentation processes result in spatial and stratigraphic heterogeneities and consequently in a complex slope architecture (Playton et al., 2010). This variability makes the development of depositional and stratigraphic models for carbonate slopes challenging.

The slopes of the Bahamian carbonate platforms in the past were in the focus of studies on carbonate slope depositional systems (Droxler et al., 1983; Droxler and Schlager, 1985; Reijmer et al., 1988; Kenter, 1990; Eberli, 1991; Grammer et al., 1993; Schlager et al., 1994; Kenter et al., 2001). During sea-level highstands, the top of a carbonate platform is occupied by a highly productive carbonate factory and the excess of sediment is exported primarily to the leeward slope (Kendall and Schlager, 1981; Schlager and Ginsburg, 1981; Hine et al., 1981). The exported sediments form margin-parallel facies belts along the slope, which are reported to show a fining towards the basin (Mullins et al., 1984; Playton et al., 2010). By contrast, during sea-level lowstands, the exposed platform top produces no sediment and the sediment supply to the slopes is restricted to pelagic input (Schlager and Ginsburg, 1981). The limited sediment supply to the slopes enables the early diagenetic formation of hardgrounds and firmgrounds (Schlager et al., 1994; Malone et al., 2001; Eberli et al., 2002).

The angle of carbonate slopes is in part controlled by the grain size of the exported sediments and the degree of submarine cementation (Schlager and Camber, 1986). Kenter (1990) showed that the angle of repose decreases with increasing mud content. Where the slope angle exceeds the angle of repose, gravity-driven processes re-adjust the slope angle. Recent studies have documented large mass-gravity flows with the potential to generate tsunamis (Mulder et al., 2012; Jo et al.,

* Corresponding author.
E-mail address: marco.wunsch@uni-hamburg.de (M. Wunsch).

https://doi.org/10.1016/j.sedgeo.2017.10.013
0037-0738/© 2017 Elsevier B.V. All rights reserved.

2015; Principaud et al., 2015; Schnyder et al., 2016). Further studies demonstrate the additional influence of bottom and contour currents on slope stability and sedimentation along carbonate slopes (Betzler et al., 2014; Tournadour et al., 2015; Chabaud et al., 2016; Wunsch et al., 2016). In particular, Betzler et al. (2014) and Wunsch et al. (2016) show how platform sediment export and bottom currents sculpture the present day slopes and determine the distribution of sedimentary features along the leeward slope of Great Bahama Bank.

Here we use new high-resolution subsurface and multichannel seismic data from the southwestern leeward slope of Great Bahama Bank to trace the slope depositional dynamics resulting from of the interplay between mass gravity and current processes back in time. Two stochastic facies models emphasize the influence of the slope morphology on the sediment and facies distribution. This adds new facets for a better understanding of carbonate platform slope depositional systems elsewhere.

2. Geologic and oceanographic setting of the study area

The study area is located along the western slope of Great Bahama Bank (GBB) and covers the segment of the slope that is facing the Santaren Channel (SC). The SC is a 65 km wide and 750 m deep marine strait between GBB and Cay Sal Bank connecting the Straits of Florida with the Old Bahama Channel (Fig. 1A).

The isolated platforms of the Bahamian archipelago lie on horsts, which formed during the opening of the Atlantic (Mullins and Lynts, 1977; Eberli and Ginsburg, 1987; Eberli, 1991). Although the initial relief was partly leveled during early platform coalescence, tectonic segmentation during the collision of the North American plate with the Cuban arc reactivated older faults, drowned part of the platforms and created seaways (Eberli and Ginsburg, 1987; Ladd and Sheridan, 1987; Masaferro and Eberli, 1999). During the Neogene, a renewed coalescence of several smaller platforms by seaway filling and bank progradation formed the modern GBB (Eberli and Ginsburg, 1987). Since the late Middle Miocene, the platform margin facing the SC prograded 25 km to the west (Eberli and Ginsburg, 1987). During the Pliocene, a change in the depositional profile from a ramp towards a flat-topped platform with a steep margin occurred (Betzler et al., 1999). Ball et al. (1987) proposed that the Florida Current (FC) inhibited further westward progradation of the platform margin that faces the Straits of Florida. However, an up to 90 m thick wedge of Holocene sediments indicates ongoing sediment accumulation at the slope facing the SC (Wilber et al., 1990; Eberli et al., 1997; Roth and Reijmer, 2004, 2005; Betzler et al., 2014; Wunsch et al., 2016). This Holocene sediment wedge at the leeward flank of GBB is modified by contour currents and has thus been designated as periplatform drift by Betzler et al. (2014).

The current system around the Bahamian archipelago is dominated by the North Atlantic gyre to the east of the Bahamas and by the FC to the west (Bergman et al., 2010). The FC is composed of water masses from the Gulf of Mexico and the Caribbean Sea (Schmitz and Richardson, 1991). It passes the Straits of Florida and becomes a major part of the Gulf Stream, the surface-flowing limb of the North Atlantic gyre. The FC does not fill the entire strait and coastal countercurrents flow along the Florida shelf (Neumann and Ball, 1970; Grasmueck et al., 2006). Along the northern side of CSB, the FC meanders and forms cyclonic frontal eddies. These eddies force a part of the FC to bend southwards into the Santaren Channel (Lee et al., 1995). Currents flow with a velocity of about 60 cm/s along the windward slope of CSB (Lüdmann et al., 2016) (Fig. 1A), and north directed contour currents with a speed of ca. 120 cm/s below 500 m water depth flow along the eastern flank of the SC (Leaman et al., 1995; Lüdmann et al., 2016). This current merges with the FC at the confluence of the Santaren Channel and the Straits of Florida (Fig. 1A). The west-directed surface currents are responsible for the distribution of sediments and the prevailing off-bank transport to the western leeward side of the Bahamian carbonate platforms (Hine and Steinmetz, 1984). The surface current system is the result of the interaction between ocean and trade-wind-driven currents. Numerical models indicate a prevailing west to northwest-directed surface current in the study area (Wang and Mooers, 1997; Kourafalou and Kang, 2012).

3. Material and methods

3.1. Geophysical data

Twenty-seven reflection seismic lines were acquired in 2013 during cruise M95 with R/V Meteor (Fig. 1B). The data were recorded with a 144-channel digital streamer with active length of 600 m (Hydroscience Technologies Inc., Mineral Wells, Texas, USA). The seismic array consisted of a standard and a mini GI gun (Sercel, Houston, Texas, USA) with a total volume of 3.2 l, ran at 150–180 bar. Shot interval was 12.5 m at a survey speed of 5 kn. Data were processed using ProMax (Halliburton-Landmark, Houston, Texas, USA) to zero phase, filtered in time and f–k domain, and corrected for dip and normal moveout. For stacking, a bin size of 6.25 m was selected. Finally, migration in time domain was carried out. Additionally, the M95 data set was combined with two older data sets to enhance the seismic grid. The first, a low resolution industrial survey was acquired by Geophysical Service Inc., using a 3.200 m long, 96-channel streamer and shot with a 2.015 in^3 airgun. The second data set is high-resolution survey using a 45/105 in^3 airgun and recorded with a 24-channel streamer. Details of the acquisition and processing are given in Anselmetti et al. (2000).

High-resolution subsurface data were recorded with a parametric sediment echosounder (PARASOUND P70, Atlas Elektronik, Bremen, Germany) (Fig. 1C). The system was operated with two frequencies (18 kHz and 22 kHz). The software PS32segy (Hanno Keil, University of Bremen, Germany) was used to cut and convert the data. Data processing was performed with the software package ReflexW (Sandmeier Software, Karlsruhe, Germany), comprising automatic gain control (AGC) and amplitude normalization along the profile. For visualization and interpretation, sub-bottom and reflection seismic data were loaded into Petrel E&P (Schlumberger, London, UK).

3.2. Bathymetric data

Bathymetric data were recorded with the hull-mounted Multibeam system EM122 (Kongsberg Maritime, Kongsberg, Norway), which uses a sonar frequency of 12 kHz, 432 beams and 864 soundings per ping. The system was operated with 140° sector coverage and equidistant sounding spacing. Beams were stabilized for roll, pitch and yaw. The software Caris HIPS & SIPS (Caris, Fredericton, Canada) was used for data processing and gridding (7.5 m cell size). Backscatter intensities were processed to estimate the acoustic properties of the surface sediments (c.f. Wunsch et al., 2016). The backscatter intensities were draped as a sonar mosaic onto the bathymetric grids for visualization. The software package Fledermaus (QPS, Zeist, The Netherlands) was used for data visualization and interpretation.

3.3. Stochastic facies modeling

To reconstruct lateral facies changes, stochastic modeling was performed by using the sequential indicator simulation with the software package Petrel E&P (Schlumberger, London, UK). The code is provided in the Geostatistical Software Library (GSLIB) and is based on the indicator approach (Journel, 1983; Jaime Gómez-Hernández and Mohan Srivastava, 1990; Deutsch and Journel, 1998). The indicator approach transforms each facies into a new variable, and the value of each variable corresponds to the probability of finding the related facies at a given position. This stochastic method is normally used to model heterogeneities (facies distribution, porosity, permeability) in hydrocarbon reservoirs. Input data for stochastic modeling are based on both the

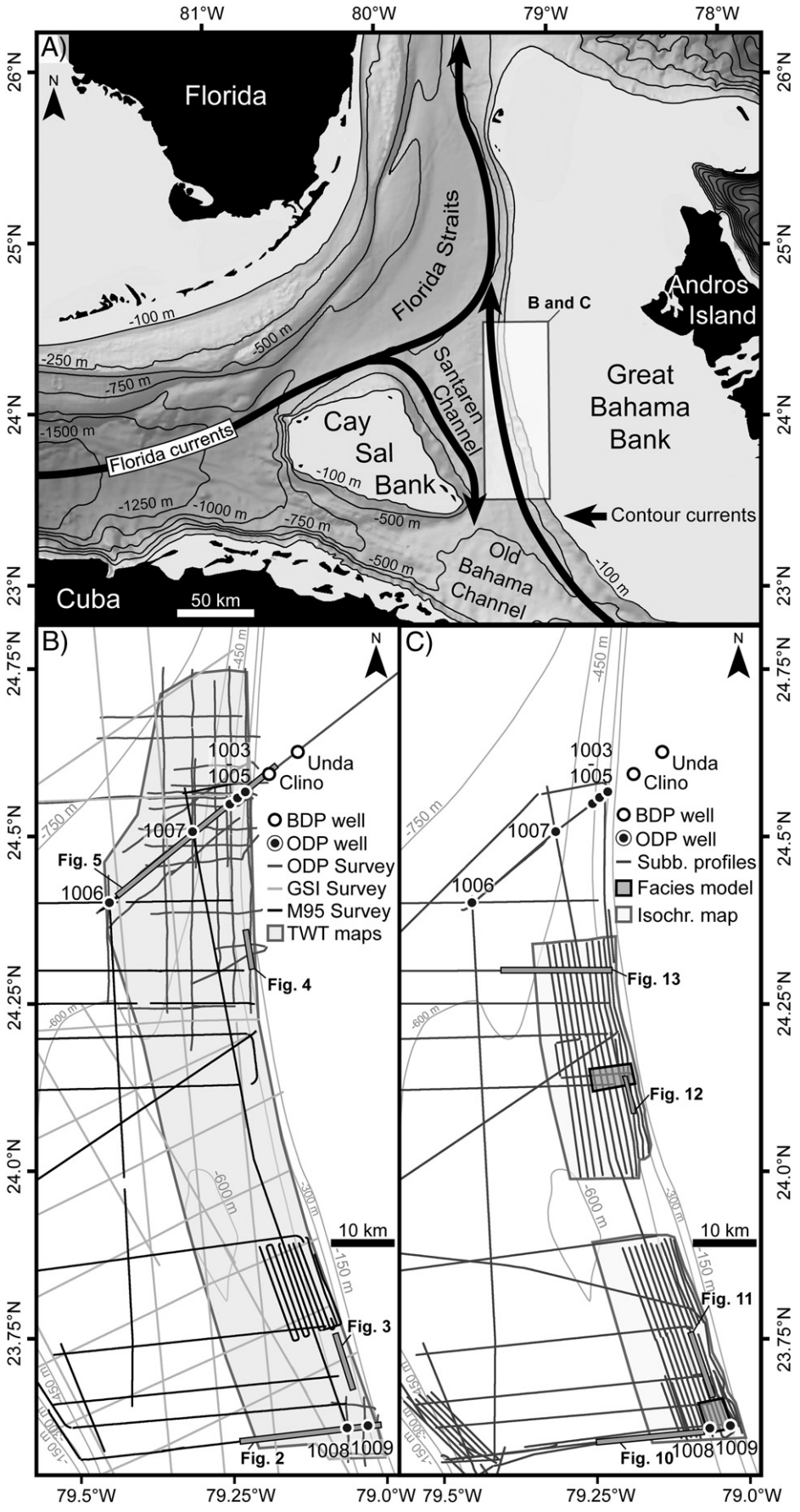
A)
Florida
Florida Straits
Santaren Channel
Florida currents
Cay Sal Bank
Great Bahama Bank
Andros Island
B and C
Contour currents
Old Bahama Channel
Cuba
50 km
-100 m
-250 m
-500 m
-750 m
-1000 m
-1250 m
-1500 m
81°W
80°W
79°W
78°W
26°N
25°N
24°N
23°N
B)
C)
1003
1005
1007
1006
Unda
Clino
BDP well
ODP well
ODP Survey
GSI Survey
M95 Survey
TWT maps
Subb. profiles
Facies model
Isochr. map
Fig. 5
Fig. 4
Fig. 3
Fig. 2
Fig. 13
Fig. 12
Fig. 11
Fig. 10
1008
1009
10 km
-450 m
-600 m
-300 m
-150 m
24.75°N
24.5°N
24.25°N
24.0°N
23.75°N
79.5°W
79.25°W
79.0°W

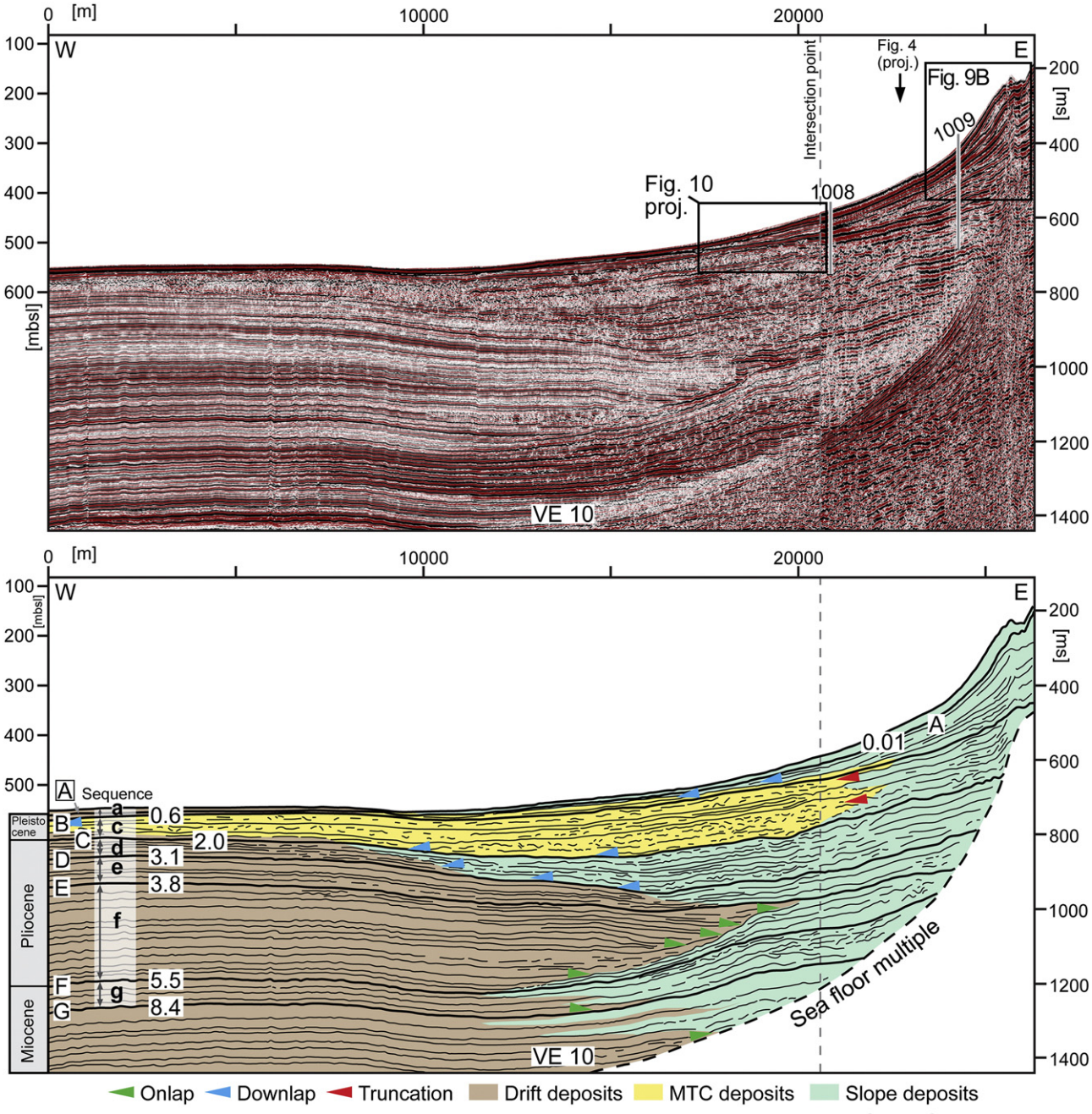

Fig. 2. Along-slope composite seismic profile from the southern working area and interpretation below. The dashed line indicates the intersection point. See Fig. 1B for location. Seven seismic sequence boundaries (SSBs) (A to G) were defined following the nomenclature of Eberli et al. (1997). The ages of the SSBs are given in million years (Ma) and were determined based on calcareous nannofossil and planktonic foraminifer events. These seismic sequence boundaries delimit seven seismic sequences (a to g). Based on the seismic reflection patterns, three major deposit types form the slope-to-basin transition. The first type, the slope deposits (green), documents the deposition of platform material onto the leeward slope. Slope deposits generally consist of inclined discontinuous to moderately continuous reflections of low to medium amplitude. Basinal deposit type is formed by drift deposits (brown). The drift deposits are part of the Santaren drift, which consists of continuous and parallel reflection of low to high amplitude. The third major deposit type is formed by the MTC deposits (yellow). The MTC deposits are generated by large slope failures and form lenticular packages with a chaotic internal refection pattern.

hydroacoustic data and the sedimentological data of ODP Leg 166 (Eberli et al., 1997) amended with grab and box core data (Wunsch et al., 2016) as well as gravity core data from Cruise M95 CICARB. Seven seismic facies were defined by correlating the sedimentological information typical the reflection patterns in the high-resolution sub-bottom data and linked to a specific sediment texture classified after Dunham (1962) and Embry and Klovan (1971). To extend the sedimentological information, synthetic wells were created. Each synthetic well

Fig. 1. A: Location of the study area. Prevailing directions of contour currents are marked with arrows. Current data after Lee et al. (1995), Leaman et al. (1995), Bergman et al. (2010), and Lüdmann et al. (2016). Box shows the outline of the study area shown in B and D. B: Study area within the Santaren Channel. Gray and black lines indicate reflection seismic profiles; ODP leg 166 sites 1003 to 1009 are marked with black, white-rimmed points; well positions of the Bahamian Drilling Program are indicated by white, black-rimmed points. Coverage of contour maps (Fig. 8) is indicated by gray shading. C: Black lines show the position of high-resolution subsurface profiles; light-gray rectangles indicate the positions of the isochore maps (Fig. 14); dark-gray rectangles show the positions of the stochastic facies models (Figs. 16; 17).

provide an interpretation of the sedimentological section based on these seismic facies.

4. Results

4.1. Major deposit types and general reflection pattern

Based on the seismic reflection patterns, Anselmetti et al. (2000) defined two major types of deposits in the slope-to-basin transition of leeward slope of the GBB: slope deposits and drift deposits. Slope deposits, consisting of inclined discontinuous to moderately continuous reflections of low to medium amplitude (Fig. 2) that strike across, appear as discontinuous subparallel reflections of low to high amplitude (Fig. 3). Channel incisions with cut-and-fill structures occur at different stratigraphic levels (Fig. 4). Texturally, the slope deposits are composed of mudstone, wackestone, packstone, and grainstone with interbedded floatstone layers that represent a wide spectrum of depositional processes, from pelagic fall-out to turbiditic flow (Eberli et al., 1997; Betzler et al., 1999; Bernet et al., 2000). Basinwards, slope deposits interfinger with the drift deposits of the Santaren drift (Bergman, 2005). In the reflection seismic data, the drift deposits are imaged as continuous and parallel reflections of low to high amplitude (Anselmetti et al., 2000) (Fig. 5). At ODP Site 1006, these drift deposits consists of mudstone or lithified mud- to wackestone with intercalated clay layers (Eberli et al., 1997).

Mass transport complex (MTC) deposits were later recognized as a third type of slope-to-basin deposits (Principaud et al., 2016). The MTC deposits form lenticular packages with a chaotic internal refection pattern, often intercalated between the slope deposits and the drift deposits (Figs. 2; 5). Cores from ODP sites 1007 and 1008 indicate that

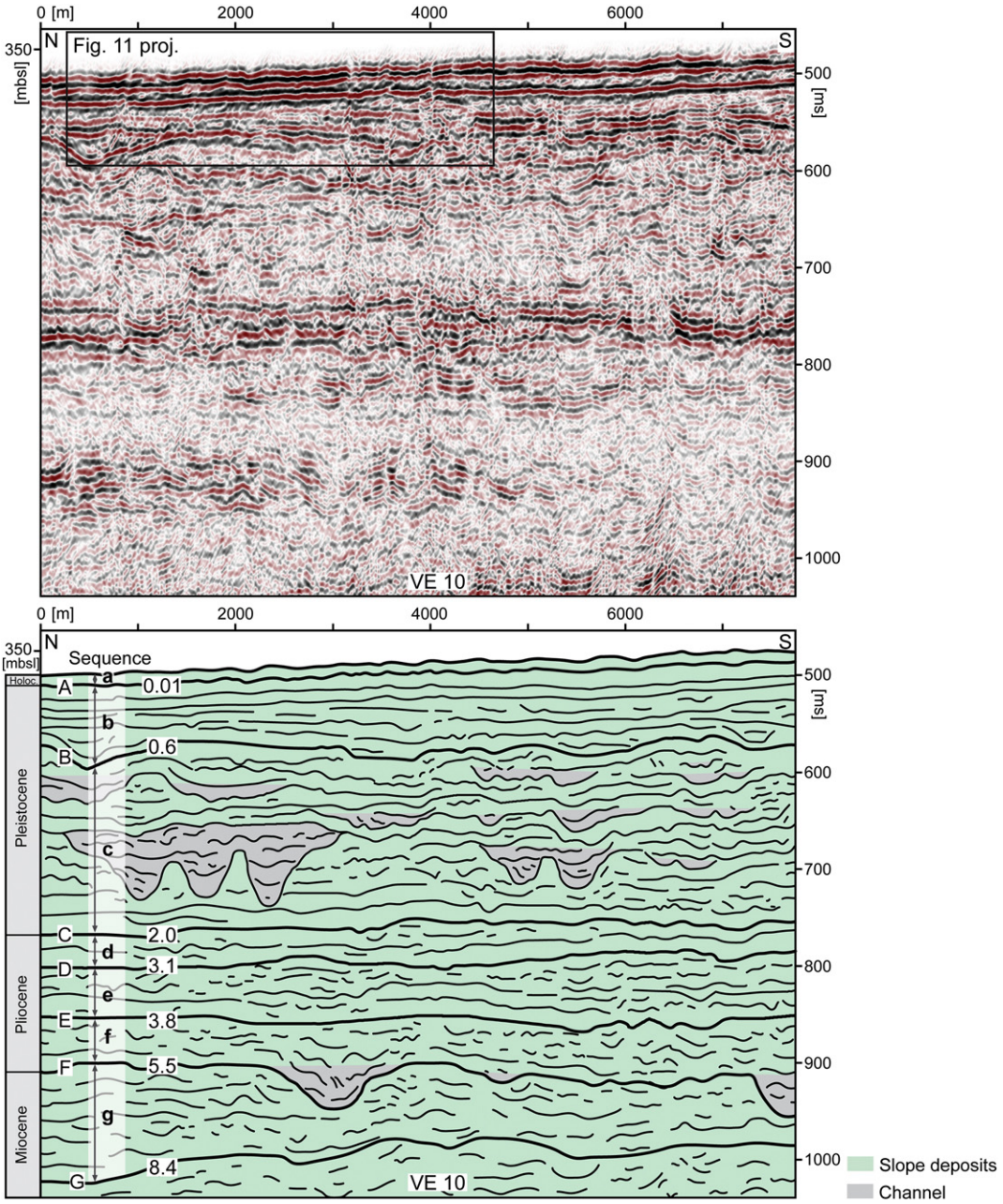

Fig. 3. Across-strike seismic profile from the southern working area and interpretation below. Profile location is indicated in Fig. 1B. Black rectangle indicates the projected position of Fig. 11. The slope deposits (green) occur as subparallel discontinuous reflections. Channels (gray) cluster along sequence boundary F and within sequence c. These channels show a divergent filling pattern.

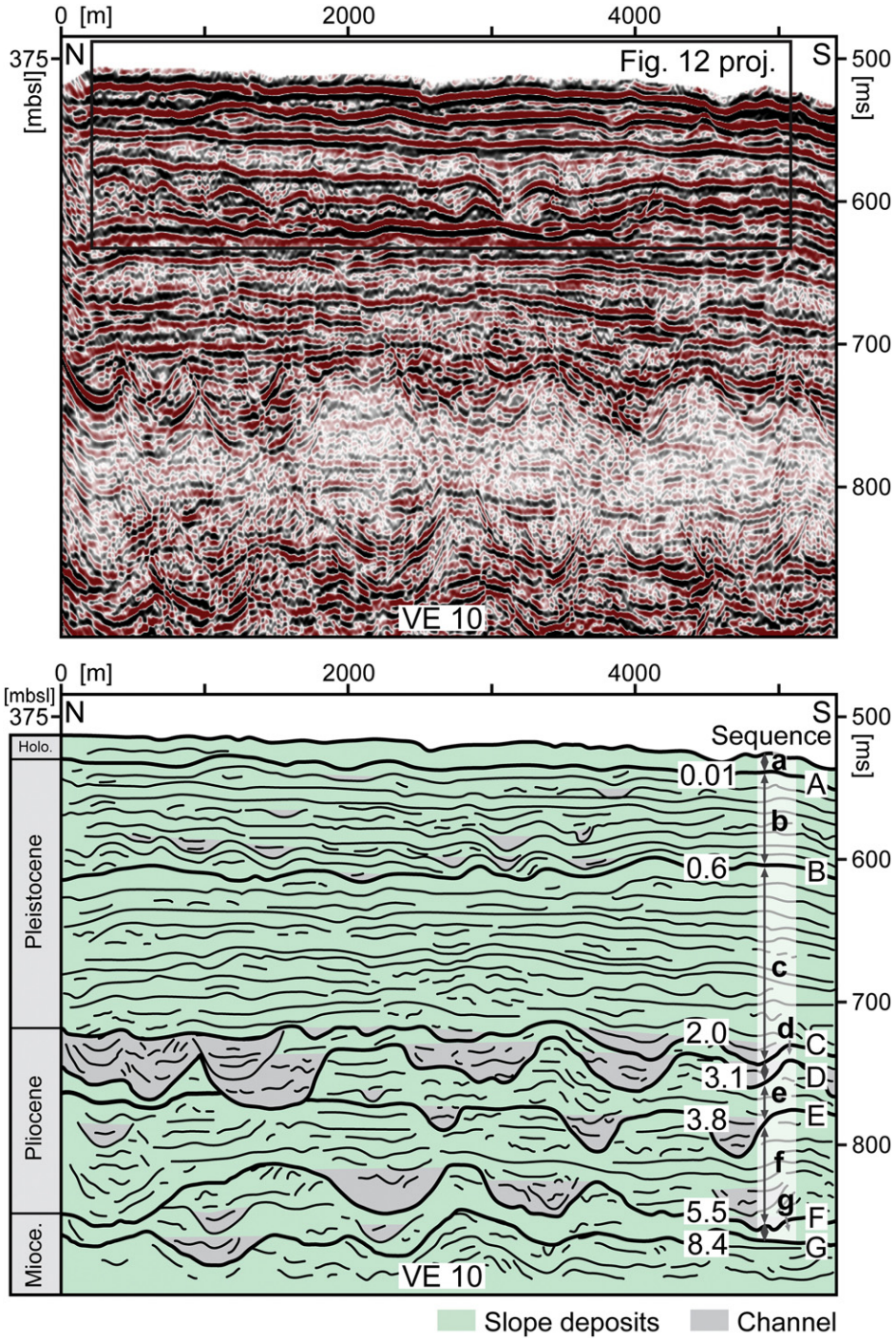

Fig. 4. Across-strike seismic profile from the northern working area and interpretation below; for location see Fig. 1B. Black rectangle indicates the projected position of Fig. 12. The slope deposits (green) occur as subparallel discontinuous reflections, which are dissected by channels (gray). Channels are more frequent along sequence boundaries G to C. Minor channel incision occurred during the formation of sequence b. The channels show a divergent to chaotic filling pattern.

these MTC deposits consist of peloidal coarse-grained and mud- to grain-dominated floatstones with slump structures (folded beds) and lithoclasts (Fig. 6) (Eberli et al., 1997; Bernet et al., 2000).

4.2. Sequence stratigraphic framework

This study concentrates on the upper seven third-order seismic sequences (g to a) and corresponding seismic sequence boundaries (SSBs) A to G defined by Eberli et al. (1997, 2002) (Figs. 2; 7A; Table 1); sea floor multiples prevent clear imaging of deeper parts of the sedimentary succession. The age assignment of the SSBs relies on calcareous nannofossil and planktonic foraminifer events (Eberli et al., 1997, 2002; Kroon et al., 2000; Wright and Kroon, 2000), herein updated to the time scale of Gradstein et al. (2012) (Fig. 7A; Table 1). The high-resolution hydroacoustic data allow describing four additional sequences of higher order (b1 to b4) within seismic Sequence b (Fig. 7B; C). These high-order sequences are delimited by prominent high-amplitude single reflections (B1 to B4) (Fig. 7B; C; Table 1). Correlation to the succession at ODP sites 1006 and 1008 corroborate that the intervals are composed of sediments with a high aragonite content and light

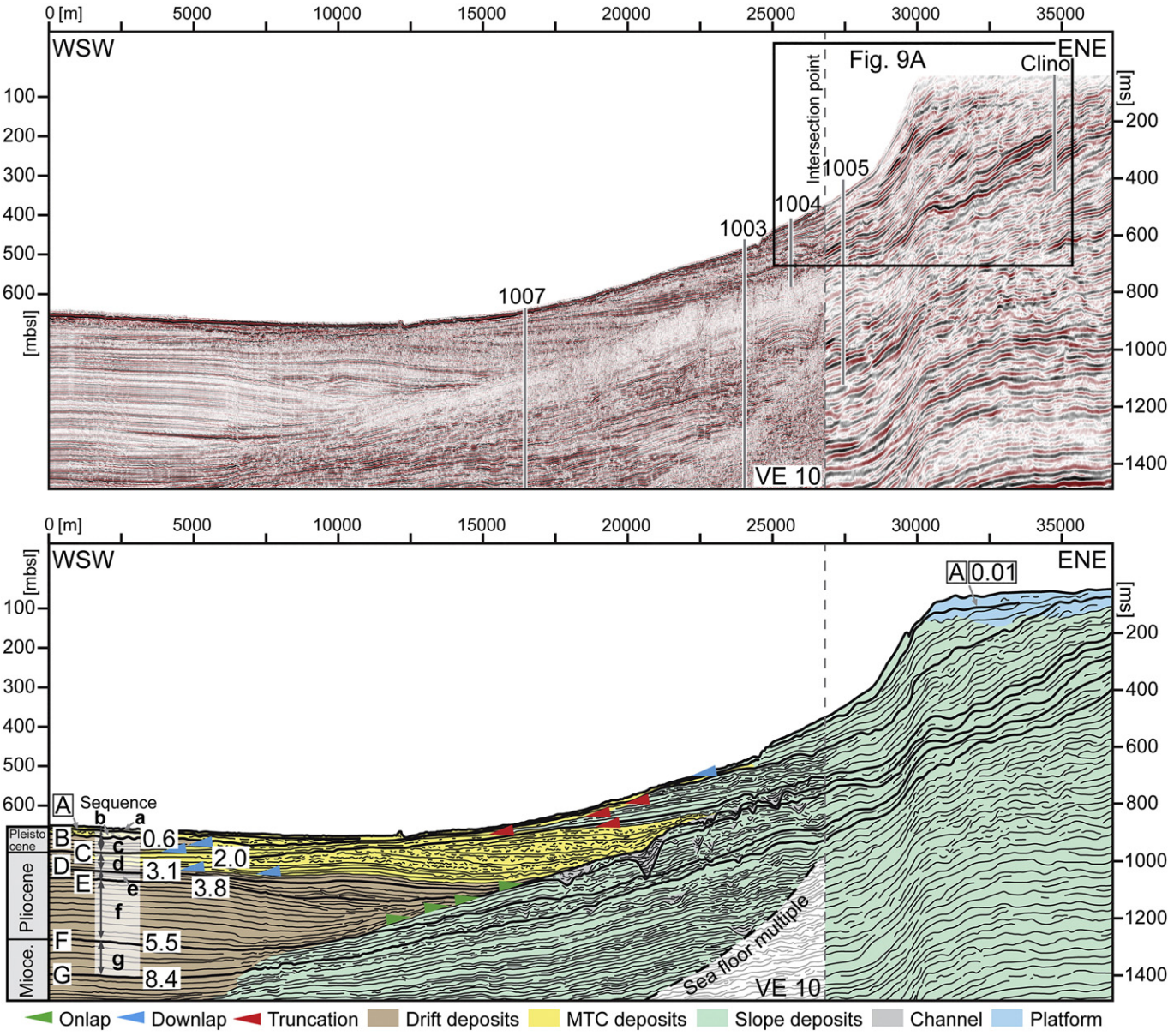

Fig. 5. Along-slope composite seismic profile from the northern working area and interpretation below. The dashed line indicates the intersection point. See Fig. 1B for location. The ages of the SSBs are given in million years (Ma). From sequence f on, the drift deposits (brown) progressively onlap and migrated eastwards accompanied by a thinning of the slope deposits (green) along the toe of slope. Major events of MTC deposit accumulation occur during the formation of sequences d to a.

stable oxygen isotopes, whereas the bounding reflections correspond to changes in sediment composition or lithification, which cause the changes in the acoustic impedance (Fig. 7B; C).

4.3. The seismic sequences

4.3.1. Sequence g

Sequence g is bounded at its base and top by seismic sequence boundary (SSB) G and F, respectively. In our data, the lower foreset and the bottomset of the prograding sequence are imaged (Fig. 2). At the toe of slope, the slope deposits gradually pass into the drift deposits (Fig. 2; 5). Slope and drift deposits show nearly the same thickness around the slope-to-basin transition (Fig. 2). In the northern part, the slope deposits thin towards the modern platform margin (Fig. 5). Minor cut-and-fill structures dissect the slope deposits in the proximal parts of the slope. Major cut-and-fill structures characterize the upper seismic sequence boundary F (Figs. 3; 4).

4.3.2. Sequence f

Sequence f is delimited at its base by SSB F, which deepens towards the west (Fig. 8A). The sequence comprises an approximately 200 m thick package of drift deposits in the basinal portion which progressively migrates eastward within the sequence while the coeval slope deposits are thin along the toe of slope (Fig. 5). The lowermost part of the succession within Sequence f interfingers with slope deposits, whereas the upper part of the drift deposits onlap the slope deposits. The migration pattern of the drift deposits varies from north to south. In the south, the internal reflections of the drift deposits show downbending onlap configurations and a continuous upslope migration (Fig. 2). In the north, the internal reflections converge towards the base of slope (Fig. 5). The drift migration and the thinning of the slope

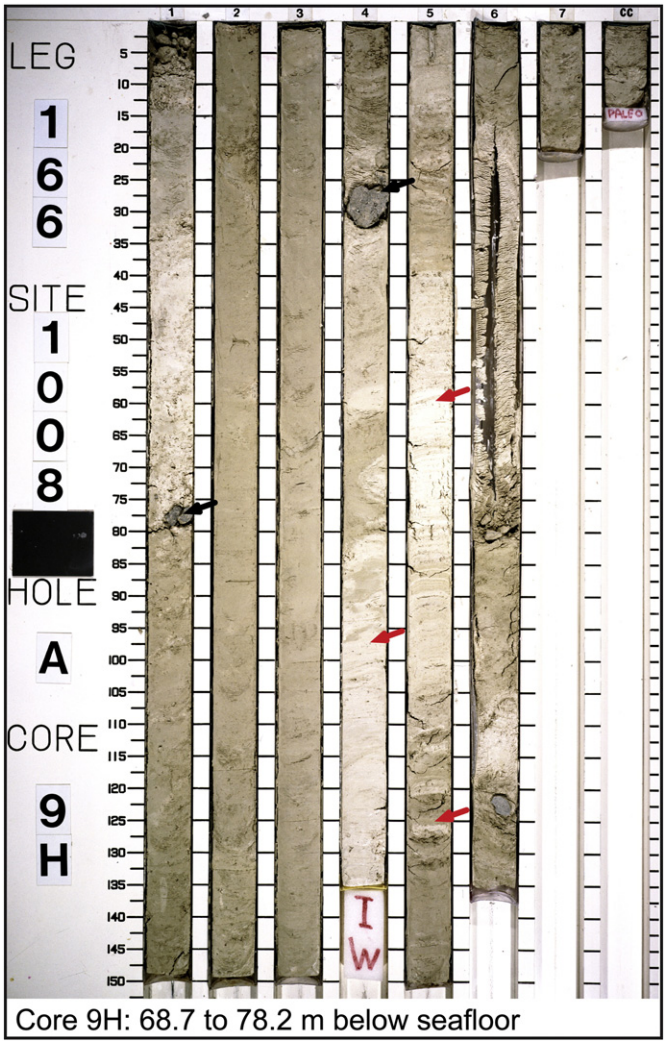

Fig. 6. Core photo from ODP site 1008A, core 9H. The core site was located in a water depth of 437 m. The upper part of the succession (Sections 1 and 2) consists of unlithified peloidal wackestone. Sections 3 to 7 consist of peloidal mudstone to wackestone. According to the biostratigraphic age model of ODP core 1008A, the sediments deposited during the Mid-Pleistocene (Eberli et al., 1997). Black arrows mark large lithoclasts. Red arrows indicate slumps structures within the sedimentary succession. Photo source: scientific party of ODP Leg 166; IODP/TAMU — Janus Web Database.

deposits along the base of slope created a north-northwest to south-southeast striking depression that shallows towards the south where migration is less pronounced (Fig. 8B).

4.3.3. Sequence e

The base of the sequence, SSB E, is an erosional unconformity with channels that cut into the underlying Sequence f (Fig. 4). These cut-and-fill structures coincide with a decrease in thickness of the slope deposits. More basinwards, the slope deposits wedge out and the mound-shaped drift deposits directly onlap SSB E. Towards the south, the slope deposits thicken and form a wedge that pass basinwards into the drift deposits (Figs. 2; 3). At the transition, both facies show nearly the same thickness (Fig. 2).

4.3.4. Sequence d

Sequence d lies above SSB D, which is irregular and forms channel-shaped incisions in the northern part of the study area (Fig. 4). These incisions coincide with large MTC deposits and a thinning of the slope deposits (Fig. 5). In dip direction, slope deposits form lenticular bodies that backfill the north-northwest to south-southeast striking depression at the toe of slope (Figs. 5; 8C). More basinwards, MTC deposits intercalate with the drift deposits (Fig. 5). Towards the south, the slope deposits form a wedge, which downlap onto the drift deposits (Fig. 2).

4.3.5. Sequence c

The lower seismic sequence boundary (SSB C) is dissected in the northern part by cut-and-fill structures and deepens towards the west and northwest (Figs. 4; 8C). In the northern part, the slope deposits form a wedge that interfinger with the MTC deposits towards the basin (Fig. 5). The internal reflections of the wedge are in parts truncated by the MTC deposits and the upper seismic sequence boundary (SSB B) (Fig. 5). In the southern part, MTC deposits partly truncate the slope deposits (Fig. 2). In the proximal parts of the slope, cut-and-fill structures of various sizes dissected the slope deposits and yielded an irregular reflection pattern (Fig. 3).

4.3.6. Sequence b

The lower bounding SSB B deepens towards the west and northwest (Fig. 8D). Sequence b forms a wedge, which intercalates with MTC deposits at the toe of slope (Figs. 2; 5). During formation of the higher order sequences b1 to b4, the platform margin prograded westward and continuously steepened (Fig. 9A). Beneath the margin, every sequence has a wedge of slope deposits with a margin-parallel ridge and an adjoined depression (Fig. 9B). Internally, every individual wedge shows the same characteristics and features but with changes along strike. These changes are also visible in the recent sea-floor morphology. In the southern part, the sea floor is occupied by a strike-continuous field of cyclic steps (Betzler et al., 2014) (Fig. 10A). In the subsurface data, the slope deposits appear as relatively transparent intervals. The seismic sequence boundaries are continuous and appear wavy in the proximal part of the wedge (Fig. 10B, C). The cyclic steps are locally interrupted by shallow furrows (Fig. 11A; B). In the margin-parallel profiles, SSB B1 and B2 appear irregular and form shallow depressions (Fig. 11B). By contrast, the overlying SBBs (B3 to B4) are flat horizons. Within sequences b3 and b4, the lower sequence boundaries are each overlain by a high-amplitude single reflection, which mimics the actual sequence boundary (Fig. 10C).

Towards the north, the sea floor is characterized by gullies and a patchy distribution of cyclic steps (Fig. 12A). The margin-parallel profiles exhibit cut-and-fill structures that cluster along the sequence boundaries (Fig. 12B). These cut-and-fill structures show a chaotic to divergent filling pattern (Fig. 12C). The abundance of these cut-and-fill structures along the SSBs leads to an irregular and discontinuous appearance of the SSBs. In some parts, the sequence boundaries B2 to B4 are truncated by SBB A, which is represented on the recent sea floor by scarps (Figs. 12B; 13A–C). At its toe, the slope is onlapped by MTC deposits, which intercalated with the drift deposits basinwards (Fig. 13B; D). This change along the strike of the slope is also visible in the isochore maps (Fig. 14). In the whole study area, Sequence b1 displays an irregular distribution, with areas of increased sediment thickness in the proximal and distal parts of the slope (Fig. 14A). In the southern part, this pattern changes during Sequences b2 to b4. The slope deposits form a distinct wedge, which thins out approximately 7 km away from the recent platform margin (Figs. 10B; 14B to D). In the northern part, the sediment distribution is intermittent and patchy in all sequences (Fig. 14A to D).

4.3.7. Sequence a

Sequence a is bordered at its base and top by SSB A and the recent seafloor, respectively. The sequence has similar characteristics as Sequences b1 to b4. To the south, it forms a smooth sedimentary wedge, which thins out approximately 7 km from the platform margin (Figs. 10; 14E). In the northern part, the sediment thickness increase in the proximal parts of the slope (Fig. 14E). In its proximal part, the slope is lined by a margin-parallel depression, which is bordered basinwards by a ridge (Fig. 9B).

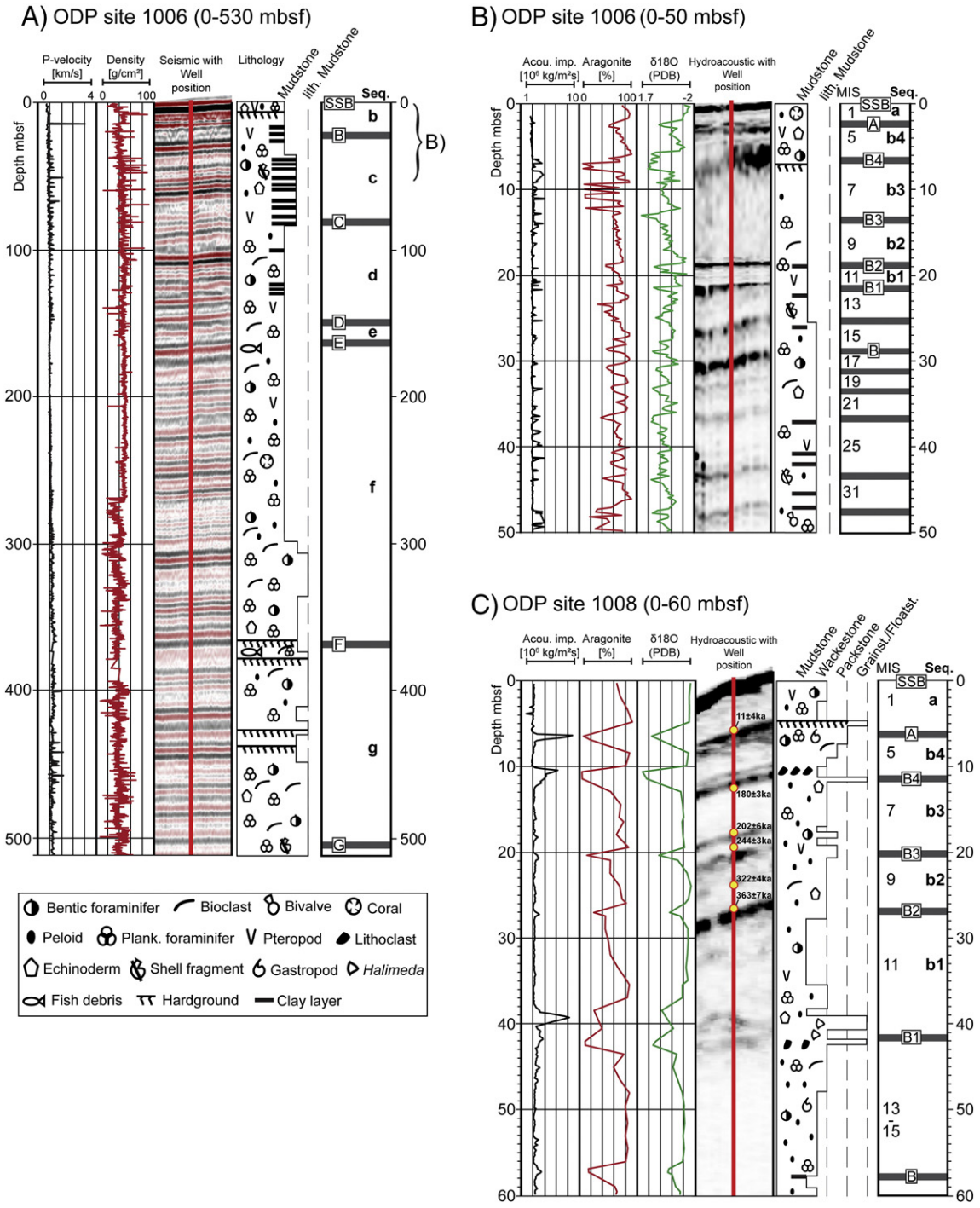

Fig. 7. Well to seismic ties of the ODP Sites 1006 and 1008. A: Well to seismic tie of ODP well 1006, which is located at a water depth of 657 m. The correlation shows that the reflections of the seismic sequence boundaries are produced by sharp changes in the sedimentary succession. In the basinal succession of ODP core, the reflections are produced by clay layers intercalated in mudstone. Density, sonic velocities and lithology column are taken from Eberli et al. (1997). B: Correlation between the subsurface data and the upper 50 m of ODP well 1006. Aragonite content and stable oxygen isotope data are taken from Kroon et al. (2000). Lithology column is from Eberli et al. (1997). C: Correlation between the subsurface data and ODP well 1008, which is located at a water depth of 437 m. Aragonite content and stable oxygen isotope data are taken from Malone (2000). Lithology column is from Eberli et al. (1997). The yellow circles indicate position of U/Th ages measured by Robinson et al. (2002) and Henderson et al. (2006).

4.3.8. Stochastic models

Sediment surface samples and core data were correlated with the high-resolution hydroacoustic data to define a series of seismic facies, which are subdivided into seismic packages and seismic surfaces (Fig. 15). The seismic facies were used to develop two stochastic models, which show the differences in the facies distribution between the northern and southern part of the slope. Both models emphasize the spatial facies heterogeneities within the sequences b1 to a. The positions of both models are indicated in Fig. 1C.

The southern stochastic model covers a slope area of 20.4 km^2 and integrates sedimentological data of ODP wells 1008, 1009, and 13 synthetic wells (Fig. 16). Within sequence b1, the facies distribution

Table 1
Summary of the seismic sequence boundaries (SSB). Ages were updated with the time scale of Gradstein et al. (2012).

SSB	Age (Ma)[a]	1003		1004		1005		1006		1007		1008		1009	
		TWT (ms)	Depth (mbsf)	TWT (ms)	Depth (mbsf)	TWT (ms)	Depth (mbsf)	TWT (ms)	Depth (mbsf)	TWT (ms)	Depth (mbsf)	TWT (ms)	Depth (mbsf)	TWT (ms)	Depth (mbsf)
A	~0.02	16	13	20	16	24	19	4	2.5	3	2	7	6	26	21
B4	~0.18	/	/	26	21	41	33	8	6	/	/	12	12.5	50	40
B3	~0.27	/	/	46	37	64	51	/	/	/	/	24	20	86	69
B2	~0.36	18	14	58	46	81	65	18	18.5	14	11	36	27	102	81.5
B1	~0.43	27	21	/	/	96	77	25	21	/	/	48	40	118	94.5
B	0.6	28	23	73	68	100	90	33	30	15	12	63	63	138	126
C	2.0	117	107	165	153	219	201	100	90	35	40	N.D.	N.D.	N.D.	N.D.
D	3.1	150	145	200	185	244	228	160	145	220	210	N.D.	N.D.	N.D.	N.D.
E	3.8	171	166	N.D.	N.D.	275	259	190	170	210	220	N.D.	N.D.	N.D.	N.D.
F	5.5	315	315	N.D.	N.D.	387	385	410	380	303	303	N.D.	N.D.	N.D.	N.D.
G	8.4	340	350	N.D.	N.D.	430	430	530	505	350	365	N.D.	N.D.	N.D.	N.D.

[a] Ages defined from biostratigraphic data, U/Th data of ODP core 1006 and 1008, respectively. / = not detected, N.D. = not drilled.

varies in downslope and along-strike direction. Sequence b1 is dominated by mudstones and packstones, which interfinger with small lenses of wackestone or wacke- to packstone. The overlying sequences (b2 to a) show a layer-cake stratigraphy along strike with little lateral facies changes. Major facies alternations occur predominantly in downslope direction. Within the sequences, the dominating facies are mudstone, mud- to wackestone, wackestone and packstone. Wacke- to packstones and pack- to grainstones and grainstones are restricted to the uppermost parts of the sequences below.

The area for the second stochastic model is located in the northern part of the study area and covers 29.8 km^2 (Figs. 1C; 17). This model integrates the sedimentological data of three gravity cores, one multicore and one box core, extended by nine synthetic wells. Compared to the model on the southern slope, the northern model exhibits a more irregular facies distribution. Rapid facies alternations occur in downslope and along-strike direction. Cut-and-fill structures form a complex pattern of isolated facies bodies, which are bounded by the SBBs. The filling of the cut and fill structures is dominated by wackestone and wacke- to packestone. Within the individual sequences, deposits are dominated by wackestones (Fig. 17), intercalated with lenses of wacke- to packstones and mud- to wackestones.

5. Discussion

5.1. Slope development since the Late Miocene

5.1.1. Sequence g (8.4 Ma–5.5 Ma)

During the Late Miocene (Tortonian), the fluctuating sea level was the main controlling mechanism for deposition and erosion along the leeward slope of Great Bahama Bank. The slope deposits are generally thicker than the basinal drift deposits, indicating that the deposition is concentrated on the slope and low current velocities (Anselmetti et al., 2000). Large erosional events, which affect the complete slope, are predominantly triggered by relative sea-level falls. A sea-level drop about 5.5 Ma ago, caused the incision of large channels along the complete leeward slope (Eberli, 2000) (Figs. 3; 4; 18A).

5.1.2. Sequence f (5.5 Ma–3.8 Ma)

Since the Messinian, the intensification of the north-directed contour currents and a contemporary increased sediment input to the basin induced an eastward migration of the Santaren drift, which started to onlap the slope deposits (Fig. 18B) (Anselmetti et al., 2000). The migration pattern of the Santaren drift varies along strike. In the

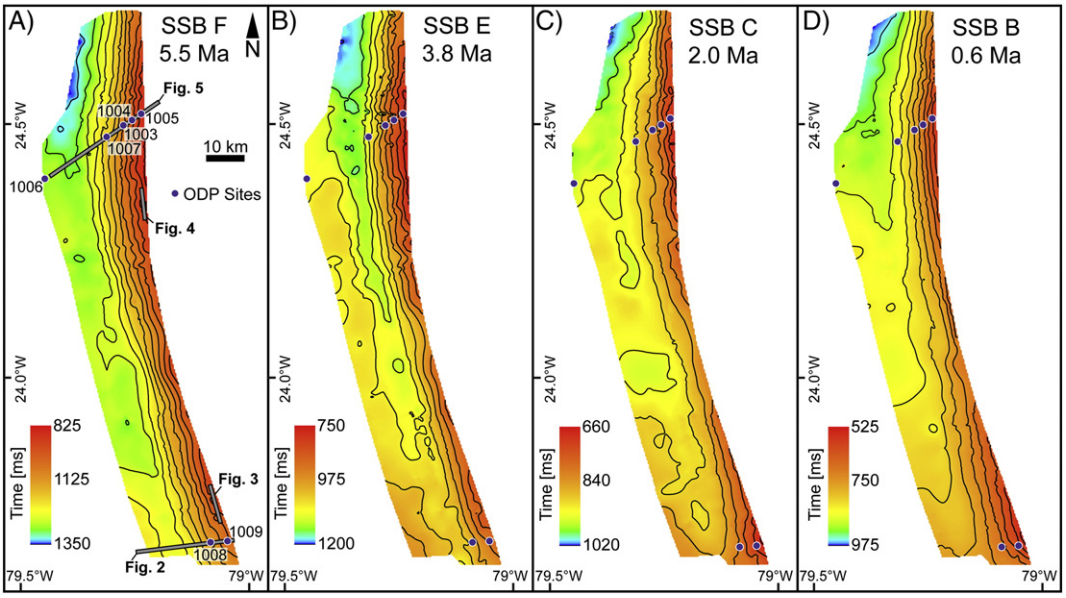

Fig. 8. Contour maps generated from the reflection seismic data by mapping the seismic boundaries F, E, C and B.

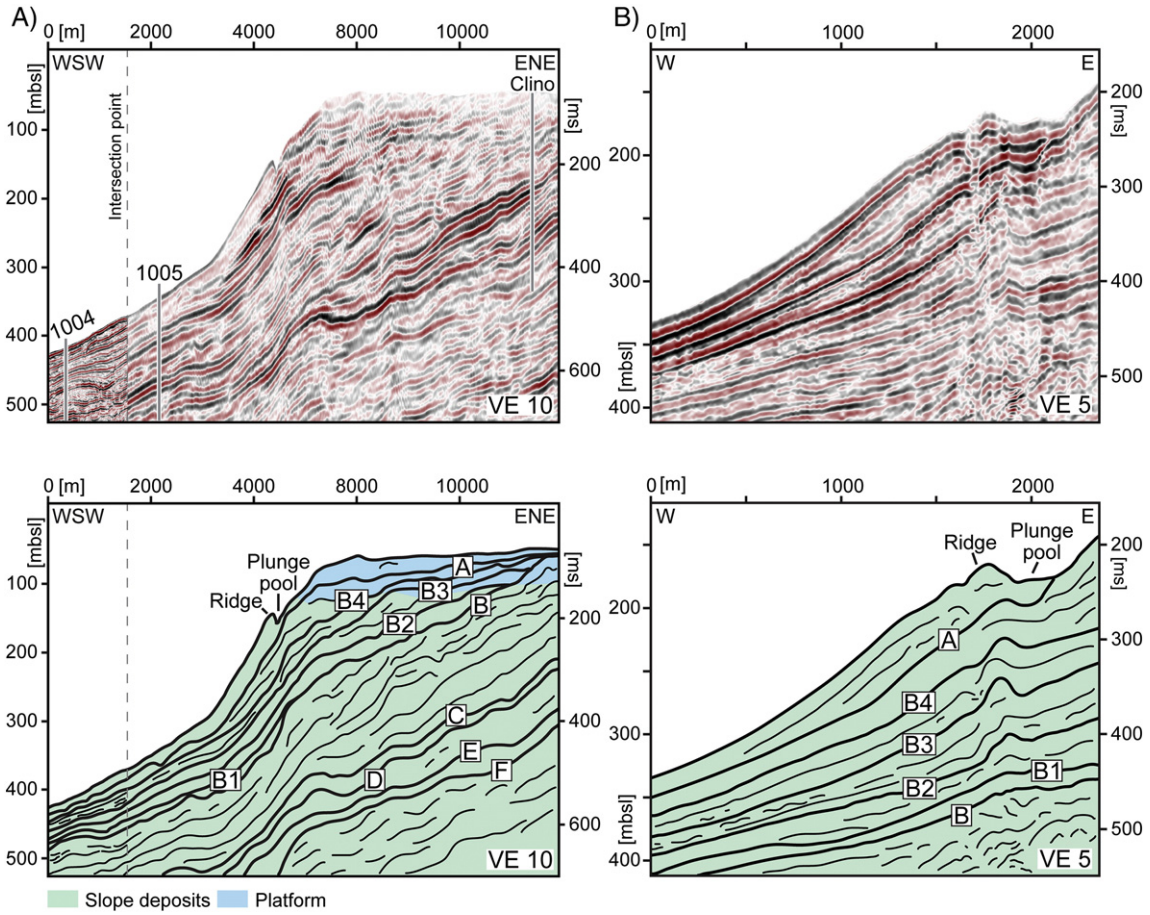

Fig. 9. A: Seismic profile from northern working area (interpretation below), which runs across the platform margin. See Fig. 6 for location. The platform margin show a continuous steepening since the onset of the sequence b, discussed in text. B: Seismic profile from the southern working area and interpretation below, see Fig. 2 for location. The profile shows a closer view on the plunge pool and adjoined sedimentary ridge. Sequence b marks the onset of the plunge pool and ridge formation, see text for discussion. The position of both structures is relatively stable since they were formed.

south, the Santaren Drift migrated continuously upslope without the formation of a deep moat. In the north, drift migration was accompanied by the formation of a deep moat along the toe of slope, restricted to the area where the north-directed contour currents of the Santaren Channel merge with the FC (Figs. 5; 8B; 18B). The drift migration is consistent with an intensification of the FC, which exceeded modern conditions (Kaneps, 1979; Haug et al., 2001; Steph et al., 2006, 2010). The intensification was caused by the gradual closure of the Central American Seaway between 4.6 and 3.6 Ma (Haug and Tiedemann, 1998). The changes in the current regime exerted an increased current control on slope architecture. During the lower Pliocene, moat indentation was accompanied by a winnowing of sediments along the toe of slope and resulting reduced sedimentation rates (Wright and Kroon, 2000). Furthermore, winnowing oversteepened the toe of slope and triggered the incision of channels that were subsequently filled with platform material (Figs. 4; 5). The continuous oversteepening of the toe of slope finally triggered headward-eroding slope failures and the incision of larger v-shaped channels (Figs. 4; 5). In the northern part, at the toe of slope, this erosional event correlates with a 0.4 Ma hiatus in the succession of ODP core 1007 (Wright and Kroon, 2000). A sea-level fall as potential trigger mechanism of the channel incision can be excluded, because the oxygen isotope data show no evidence of a major sea-level drop during this time period and the platform top was an area of high productivity (Kenter et al., 2001; Reijmer et al., 2002).

5.1.3. Sequence e (3.8–3.1 Ma)

During the early stages of Sequence e, continued eastward migration of the Santaren drift was restricted to the northern part of the study area and the drift deposits formed a smaller mound-shaped body within the moat axis (Figs. 5; 18C). This decreased rate of drift migration is likely the sedimentary expression of the contemporaneous deceleration of the FC caused by a weaker thermohaline circulation in the Northern Atlantic (Kaneps, 1979; Raymo et al., 1996; Billups, 2002). On the GBB, the Pliocene was marked by a high carbonate production and increased sediment export towards the leeward slope (Eberli et al., 1997; Reijmer et al., 2002). In the south, this led to an extensive westward progradation of the slope deposits, which suppressed eastward drift migration (Fig. 2). In the north, increased sedimentation rates on the leeward slope leveled the pre-existing channel topography (Betzler et al., 1999; Anselmetti et al., 2000). In the late stages of the sequence development, between 3.6 and 3.2 Ma, the FC gradually accelerated and recovered to its present strength caused by the onset of the Northern Hemisphere glaciations (Kaneps, 1979; Raymo et al., 1992; Haug and Tiedemann, 1998). Triggered by the re-intensification of the FC, sediment winnowing resumed along the northern toe of slope. This winnowing caused the incision of large channels around 3.1 Ma (Figs. 4; 5; 18C).

5.1.4. Sequence d (3.1–2.0 Ma)

During the late Pliocene and early Pleistocene, the moat was filled with MTC deposits, which formed a strike continuous belt (Figs. 5; 18D) (Reijmer et al., 2002; Principaud et al., 2016). The re-enforced FC caused a toe of slope backstepping, which triggered these mass-wasting processes. The MTC deposits consist of material derived from the upper slope and platform margin, funneled by the channels, which were incised around 3.1 Ma (Eberli et al., 2004; Principaud

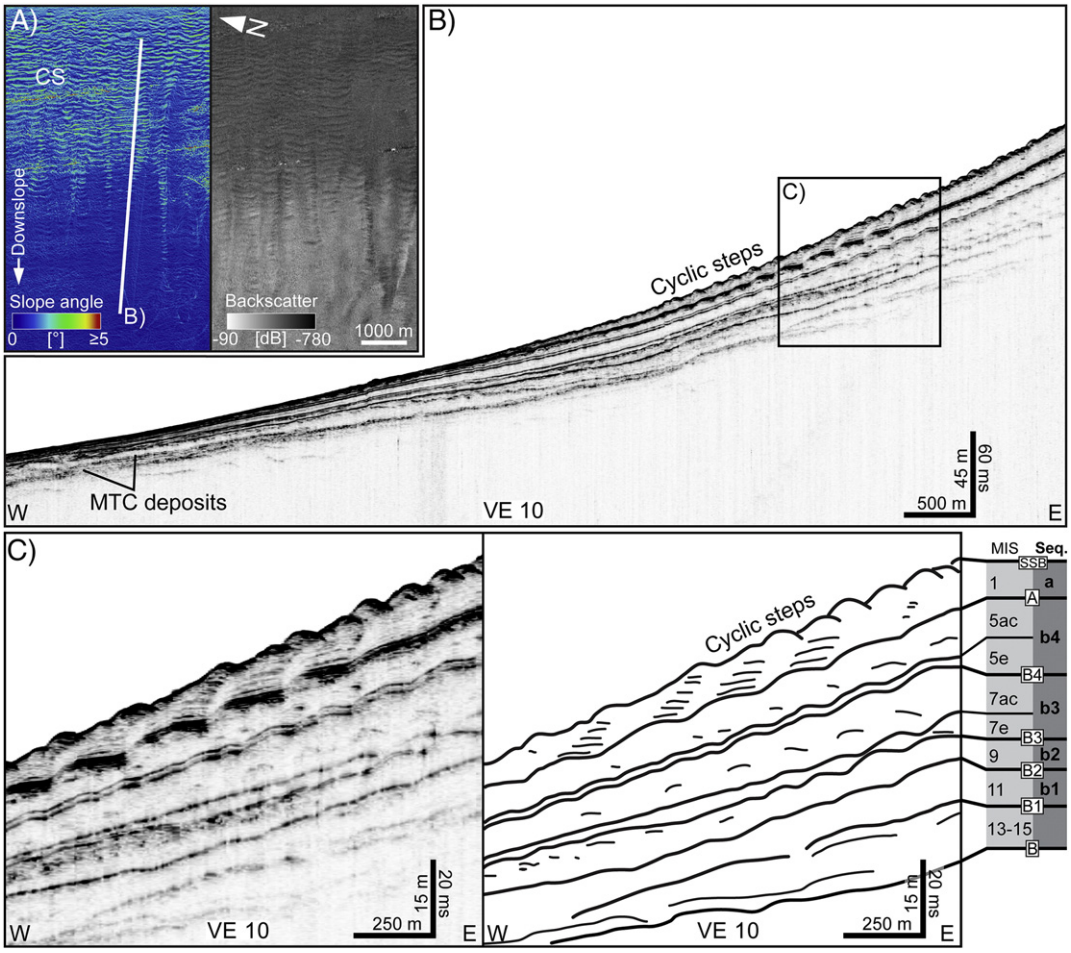

Fig. 10. A: Slope-angle steepness map and backscatter image of the southern part of the leeward slope, showing a field of cyclic steps. White line indicates the position of the subsurface profile in B. B: Along-slope high-resolution subsurface profile from the southern working area; for position see Fig. 1C. The slope deposits occur as relatively transparent wedges, which are separated by high-amplitude reflections. The wedges pinch out nearly at the same position. C: Each wedge represents a high-frequency sequence, which formed during a distinct Marine Isotope Stage (MIS) (see text for discussion). The high-amplitude reflections define the sequence boundaries. In the more proximal parts of the slope, these sequence boundaries appear wavy by the occurrence of cyclic steps.

et al., 2016). The deposition of the MTC deposits stopped after the moat was backfilled and the slope profile was leveled (Figs. 8C; 18D). The coarse-grained nature of the MTC deposits prevented the incision of a new moat. At the same time, the southern part of the leeward slope underwent extensive progradation (Sequence d; Fig. 2). This progradation coincides with a transition in the platform geometry from a carbonate ramp to a flat-topped platform (Fig. 5) (Eberli and Ginsburg, 1987; Betzler et al., 1999).

5.1.5. Sequence c (2.0–0.6 Ma)

The early Pleistocene was characterized by extensive progradation of the bank edge (Figs. 5; 9A). In the southern part, this progradation was accompanied by large slope failures, which formed a gullied upper slope and displaced slope material to the lower slope and toe of slope (Figs. 2; 3; 6; 18E). It is proposed that these slope failures were triggered during drops in sea level after times of high slope sedimentation rates. Emplacement of these deposits coincides with the Mid-Pleistocene transition (MPT). During the MPT (1.25–0.7 Ma), sea-level variability increased in amplitude, forced by the progressively change from low- 41 ka to high-amplitude 100-ka climate oscillations (Shackleton and Opdyke, 1976; Pisias and Moore, 1981; Clark et al., 2006; Maslin and Brierley, 2015). On the inner platform, sea-level variations resulted in the formation of several exposure horizons in the sedimentary succession (Kievman, 1998).

In the north, the wedge of the slope deposits reached the position of the former moat (Fig. 5). A further progradation, however, was prevented by the northward flowing contour currents, which winnowed the sediments along the toe of slope (Rendle and Reijmer, 2002). Here, the biostratigraphic data of ODP core 1007 indicate a condensed Pleistocene interval (Wright and Kroon, 2000). About 0.6 Ma ago, during a sea-level lowering, a large slope failure occurred in the northern part of the study area (Fig. 18E). This slope failure originated at the lower slope and formed a scarp (headwall), which is traceable in the entire northern part of the study area (Figs. 13B; C; 18E). This slope failure removed sediments from the lower slope and deposited the material as MTC at the base of the slope and in the adjoined basin (Fig. 13B; C). Larger slope failures that occurred at the same time along the northwestern part of the leeward GBB-slope were related to a lowering of the sea level (Wunsch et al., 2016).

5.1.6. Sequence b and a (0.6–0 Ma)

During the early formation stages of sequence b, about 0.43 Ma ago, large slope failures occurred along the entire leeward slope of GBB. It is proposed that these slope failures were triggered by changes in the amplitude of the sea-level fluctuations that occurred during the Mid-Brunhes event (MBE). The MBE roughly corresponds to the transition between MIS 12 and MIS 11 (Termination V) and marks the onset of a step-like change in the intensity of interglacial, which resulted in increased amplitude of glacial–interglacial cycles (Berger and Wefer, 2003; EPICA Community, 2004).

The post-MBE slope succession can be subdivided into five individual sedimentary wedges, based on the hydroacoustic data. These wedges

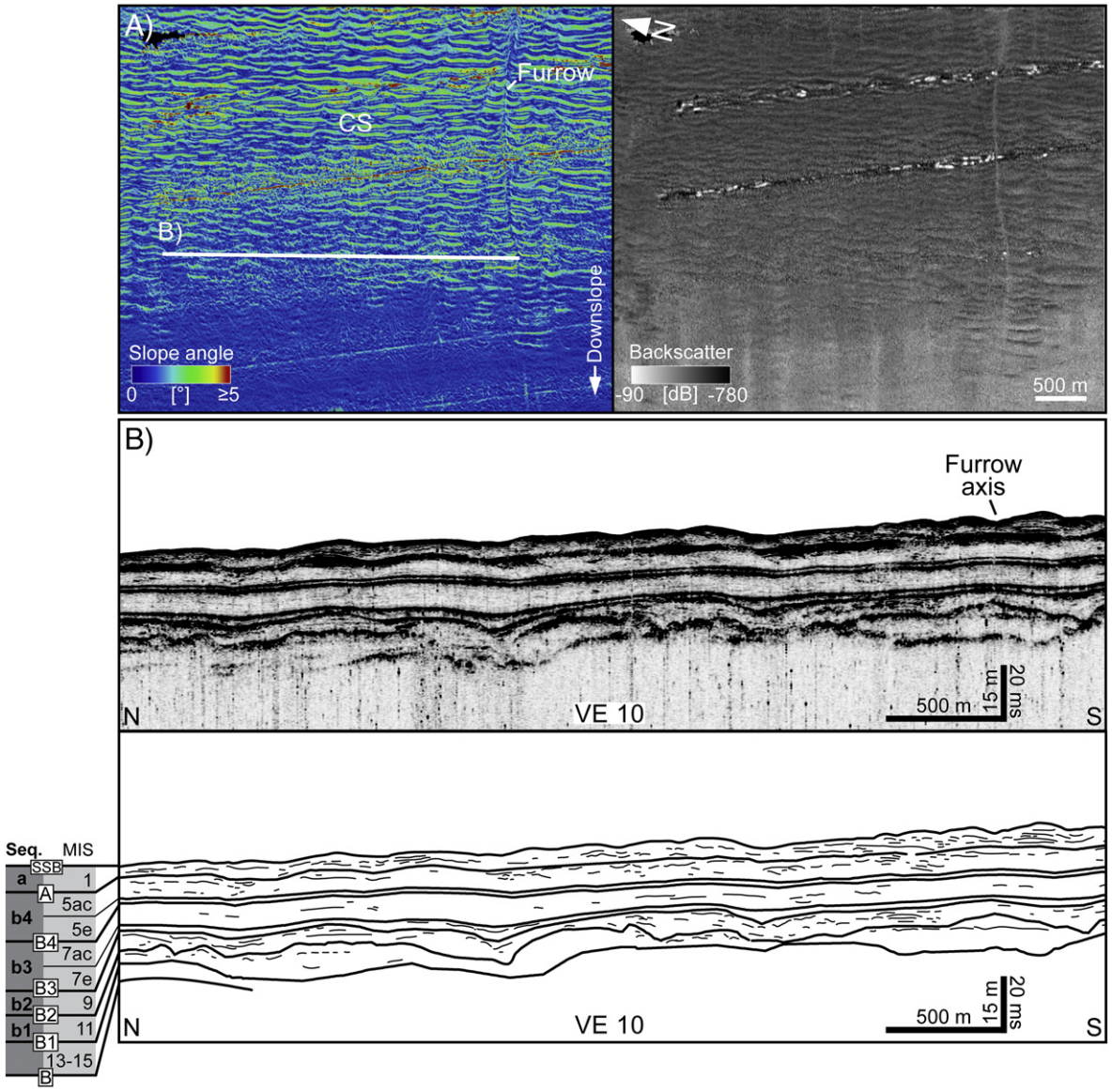

Fig. 11. A: Slope-angle steepness map and backscatter image of the southern part of the leeward slope, showing a shallow furrow cutting into a field of cyclic steps. White line indicates the position of the subsurface profile in B. B: Across-strike high-resolution subsurface profile from the southern working area (interpretation below). See Fig. 1C for position.

represent the sedimentary product of fourth-order sequences (b1 to a), generated by 100 ka glacial-interglacial cycles (Fig. 10B; C). Each of these high-frequency sequences can be assigned to a specific MIS (Figs. 7B; C). According to Wunsch et al. (2016), individual wedges can be subdivided into two parts based on sediment texture and aragonite content. The lower part represents the initial wedge, which formed right after the onset of platform flooding. Sediments are fine-grained with a higher aragonite content. The upper part of the wedge consists of coarser sediments with lower aragonite content and accumulated after completion of platform flooding (Fig. 7B; C). The individual wedges (b1 to a) differ between the northern and southern part of the study area.

5.1.6.1. Southern part of the study area. In the southern part, the lower most sequence (b1) is characterized by leveling of the slope morphology, which was formed by extensive mass wasting processed during the MBE. During the deposition of sequences b2 to a, the exported platform sediments formed individual wedges that all thin out at nearly the same distance from the recent platform margin (Fig. 10B, 18F). A further westward progradation of these highstand wedges is herein proposed to have been prevented by the north-directed contour currents that winnow the sediments along the toe of slope.

Platform-derived sedimentation on the slope is strongly tied to short-term sea-level fluctuations (Droxler and Schlager, 1985; Rendle et al., 2000). On a flat-topped carbonate platform, like the GBB, a sea-level drop of just 10 m can emerge large parts of the platform interrupting the sediment export to the slope (Schlager et al., 1994; Kievman, 1998). During sea-level lowstands, the sedimentation on the slope is reduced with deposition of coarse-grained sediments, partly enriched in lithoclasts (Fig. 7C) (Rendle-Bühring and Reijmer, 2005). Such sea-level fluctuations occurred during the MIS substages 7d (sequence b3) and 5e (sequence b4). Due to a lower sea level during MIS 7, approximately 18 m below its present position, large parts of the platform top were emerged and carbonate production was restricted to the deeper margin areas (c.f. Kievman, 1998; Manfrino and Ginsburg, 2001). Between 235 and 220 ka BP, during MIS substage 7d, sea level dropped to about 85 m below its present position. At this time, a partially

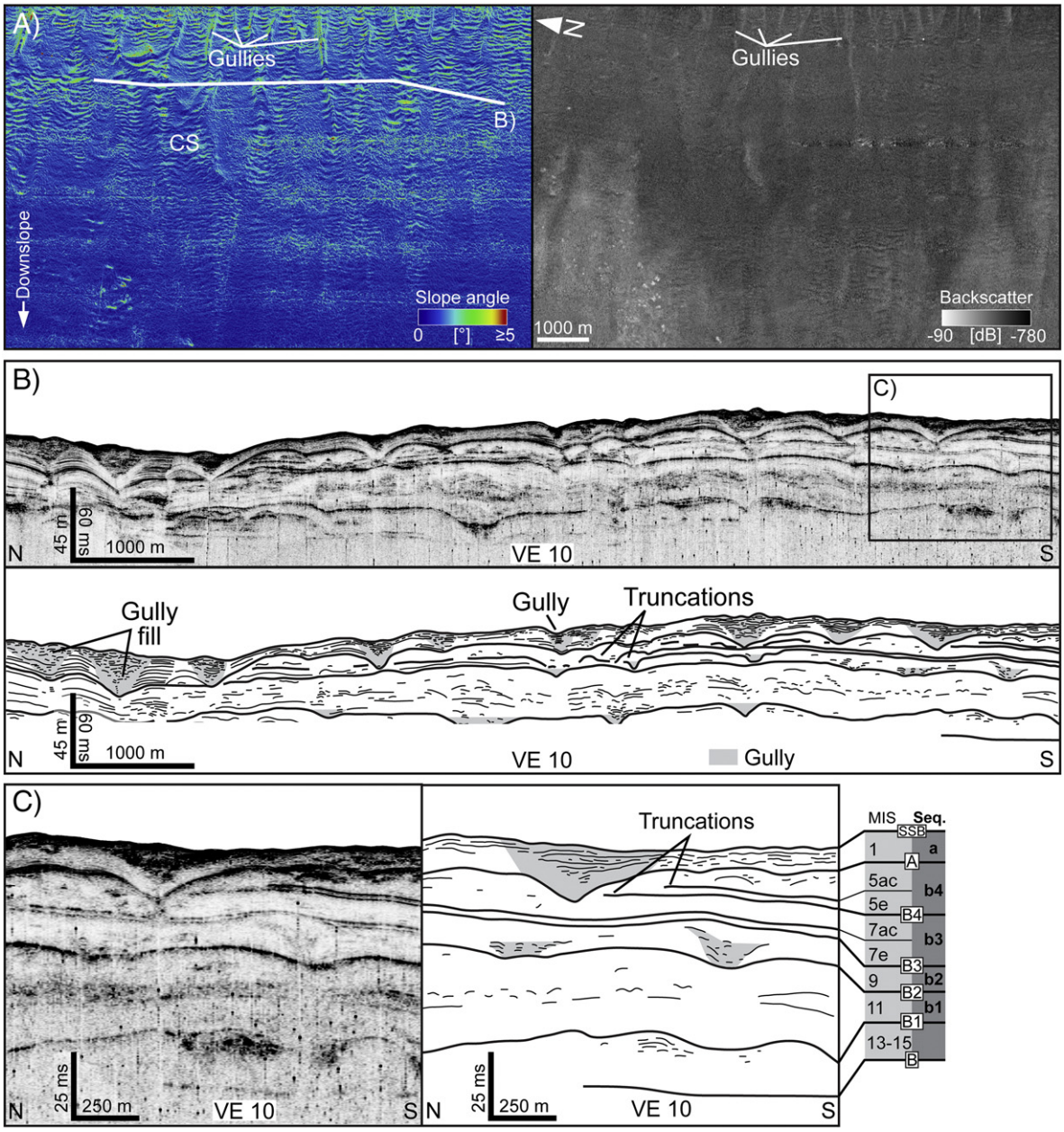

Fig. 12. A: Slope-angle steepness map and backscatter image of the northern part of the leeward slope, CS = cyclic steps. White line indicates the position of the subsurface profile in B. B: Across-strike high-resolution subsurface profile (interpretation below) from the northern working area. See Fig. 1C for position. The slope deposits are dissected by cut-and-fill structures of variable size. C: These numerous erosional features result in truncations and a noncoherent reflection pattern.

lithified wacke- to packstone interval formed along the leeward slope of GBB (Fig. 7C). After 220 ka BP, during MIS substage 7c, the margin areas were re-flooded and the carbonate production resumed.

This interpretation is supported by U/Th dates of core 1008A from depths of 17.49 and 18.84 mbsf that assign the sediments above and below the wacke- to packstone interval to the MIS substages 7c (202 ka BP) and 7e (244 ka BP), respectively (Fig. 7C) (Robinson et al., 2002; Henderson et al., 2006). A sea-level oscillation during substage 5e caused the formation of a mud- to wackestone layer enriched in lithoclasts (Fig. 7C). This sea-level oscillation lasted 10 ka, from 130 to 120 ka BP and in the Bahamian region, the sea level dropped from 2.5 m above to 2 m below its present position. Around 120 ka BP (substage 5e), after a period of continuous rise, sea level reached 6 m above its present position (Neumann and Hearty, 1996; Hearty, 1998; Hearty et al., 2007). On the GBB, this was a time of marine erosion, which dramatically reshaped the morphology of the platform top (Hearty and Neumann, 2001).

5.1.6.2. Northern part of the study area. In the northern part of the working area, the sedimentary record of the individual sequences (b1 to a) appears incomplete. This is caused by a interplay of depositional and erosional processes (Wunsch et al., 2016). Erosion primarily took place during lowerings of sea level. Slope failures eroded large volumes of sediments deposited during the previous sea-level highstand and the displaced debris were deposited as MTC at the toe of slope (Fig. 13B, 18F). These slope failures formed large depressions which upslope were bordered by head scarps, which created the initial base of gullies (Fig. 12B). During the subsequent sea-level rise and highstand, the

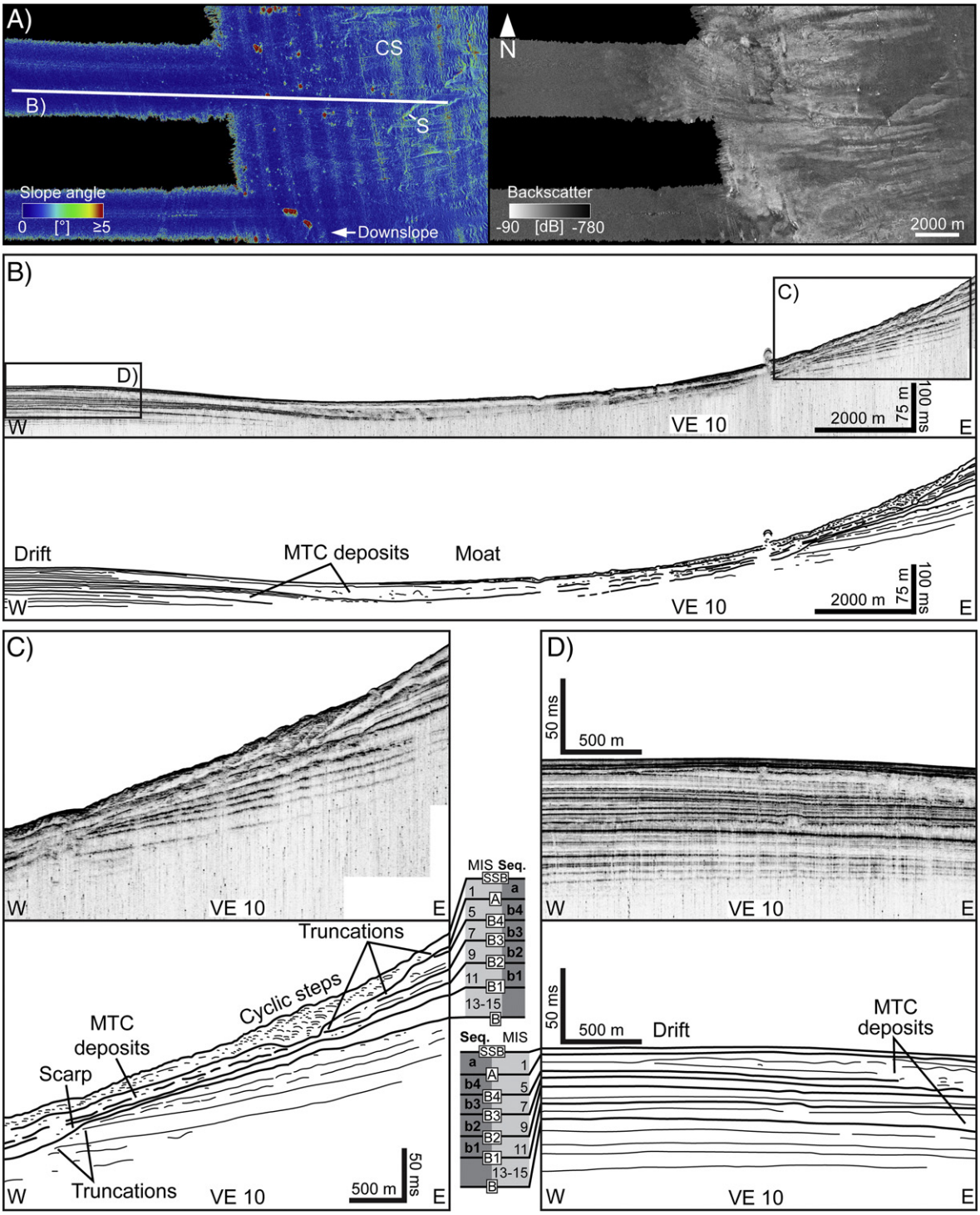

Fig. 13. A: Slope-angle steepness map and backscatter image of the northern part of the leeward slope. White line indicates the position of the subsurface profile in B. B: Along-slope high-resolution subsurface profile (interpretation below) from the northern working area. See Fig. 1C for position. C: At the lower slope, MTC deposits interfinger with slope deposits. Large buried scarps occur along the slope and truncate several sequence boundaries. D: Basinwards, the MTC deposits interfinger with drift deposits.

sediments exported from the platform were funneled by these gullies. These funneled sediments subsequently filled the depressions beneath the scarps (Figs. 13B; C; 18F). This alternating pattern of deposition and mass wasting formed a complex slope morphology of gullies and scarps, which also characterizes the recent sea floor (Figs. 12A; 13A).

5.1.6.3. Development of the recent platform margin. Since the Middle Pleistocene (sequences b1), the platform margin shows a continuous steepening, which resulted in a 150-m high recent submarine cliff (Fig. 9A). Eberli (2000) related this steepening to the increased amplitudes in the sea-level fluctuations after the MBE. It is proposed that the steepening of the margin changed the predominant mode of off-bank transport from normal off-bank currents to density cascading. Density cascading events are hyperpycnal off-bank flows triggered by the increased density of inner bank waters. Density cascading is responsible for the gross of the modern off-bank transport (Wilson and Roberts, 1992, 1995). As a result of this change in the off-bank sediment

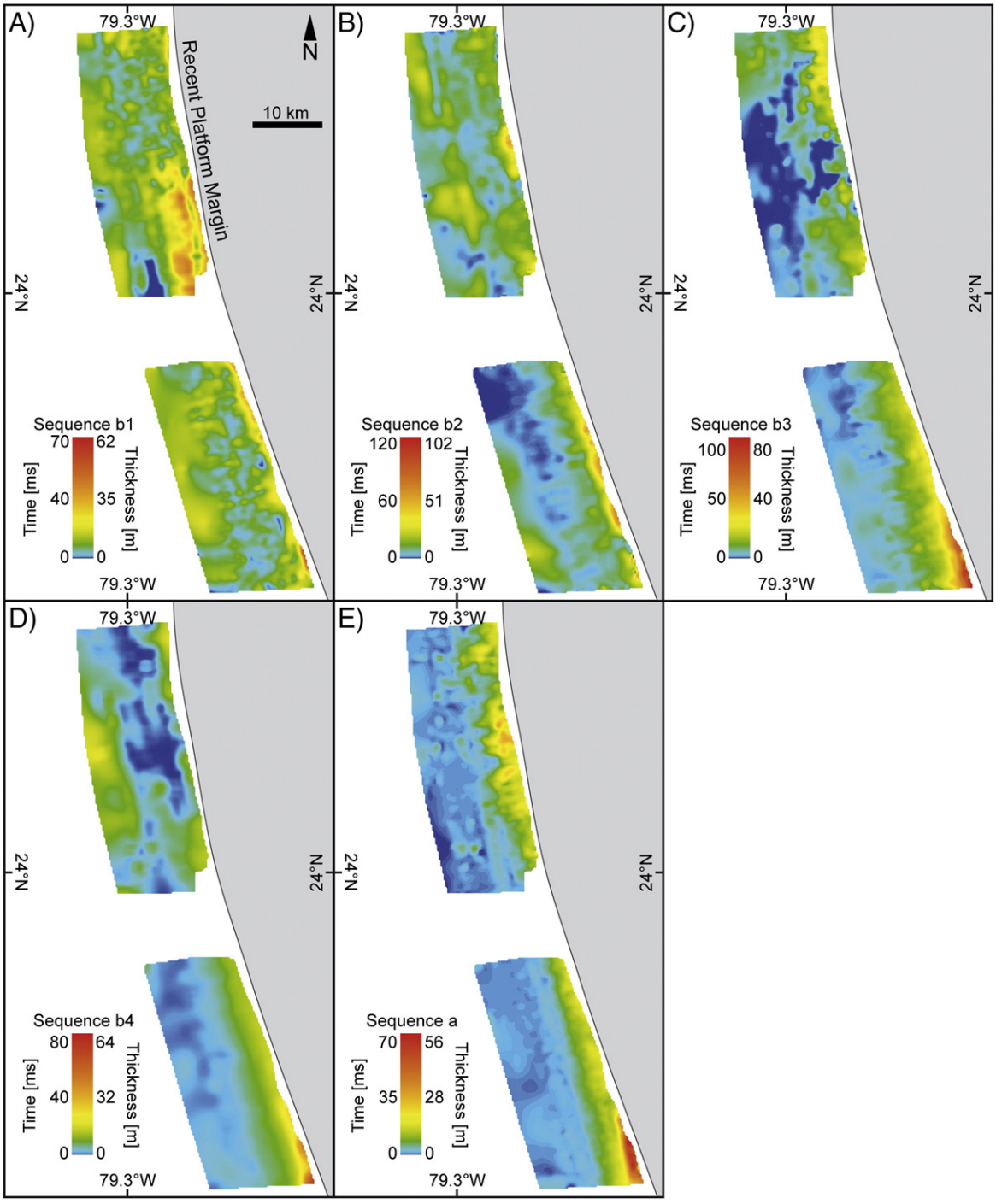

Fig. 14. Isochore maps of the high-frequency sequences b1–4 and a, generated from hydroacoustic data.

transport, two features developed that are prominent on the recent slope. The first, a margin-parallel depression, which is bordered basinwards by a sediment ridge (Fig. 9B); and the second, is the cyclic steps that occupy the complete middle slope (Betzler et al., 2014; Wunsch et al., 2016) (Figs. 10A; 11A; 18F). The margin-parallel depression represents an erosional trough, similar to a plunge pool (Wilber et al., 1990). This plunge pool was carved into the slope by the hyperpycnal flows of the density cascading, which can reach a maximum down-slope velocity of 2.47 m/s (Wilber et al., 1993). Since its initial formation, the position of the plunge pool is relatively stable (Fig. 9B). The cyclic steps formed near a slope break which has been proposed to trigger a hydraulic jump in the supercritical flows of the density cascading (Fig. 10A) (Betzler et al., 2014).

5.2. Facies distribution and heterogeneities along the leeward slope

The current influence on the GBB slope strengthens from south to north. This results in contrasting facies-distribution patterns. Currents as a driver of facies variability adds a further mechanism to the established models of carbonate slope deposition (Schlager and

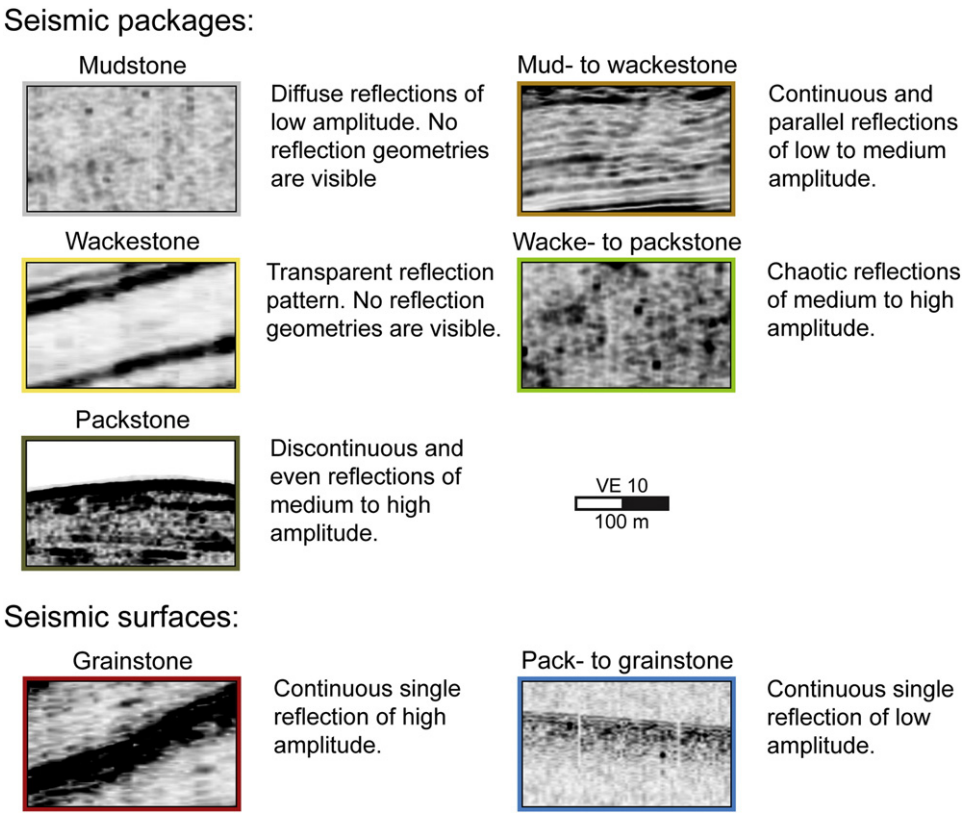

Fig. 15. Seismic facies generated from the correlation of sedimentological core data and the high-resolution subsurface data. The seismic facies are subdivided into seismic packages and seismic surfaces. See text for discussion.

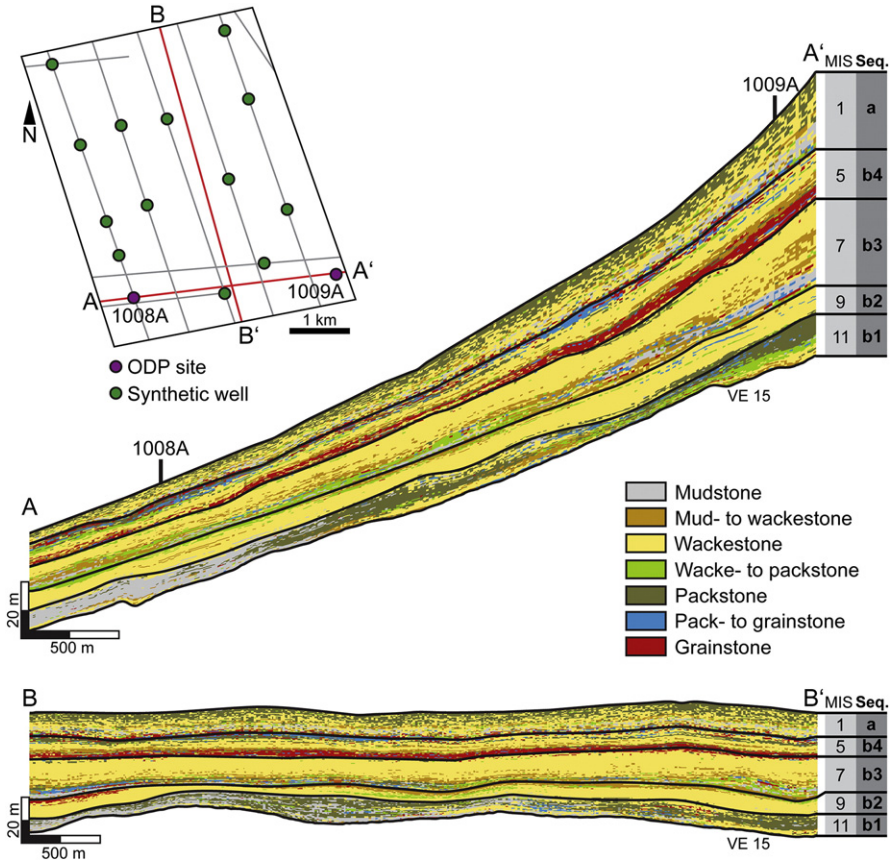

Fig. 16. Stochastic facies model for the southern study area (see location in Fig. 1C). The model shows the facies heterogeneities along-slope and across strike of the slope within the succession of the sequences b1–b4 and a. MIS = Marine Isotope Stage.

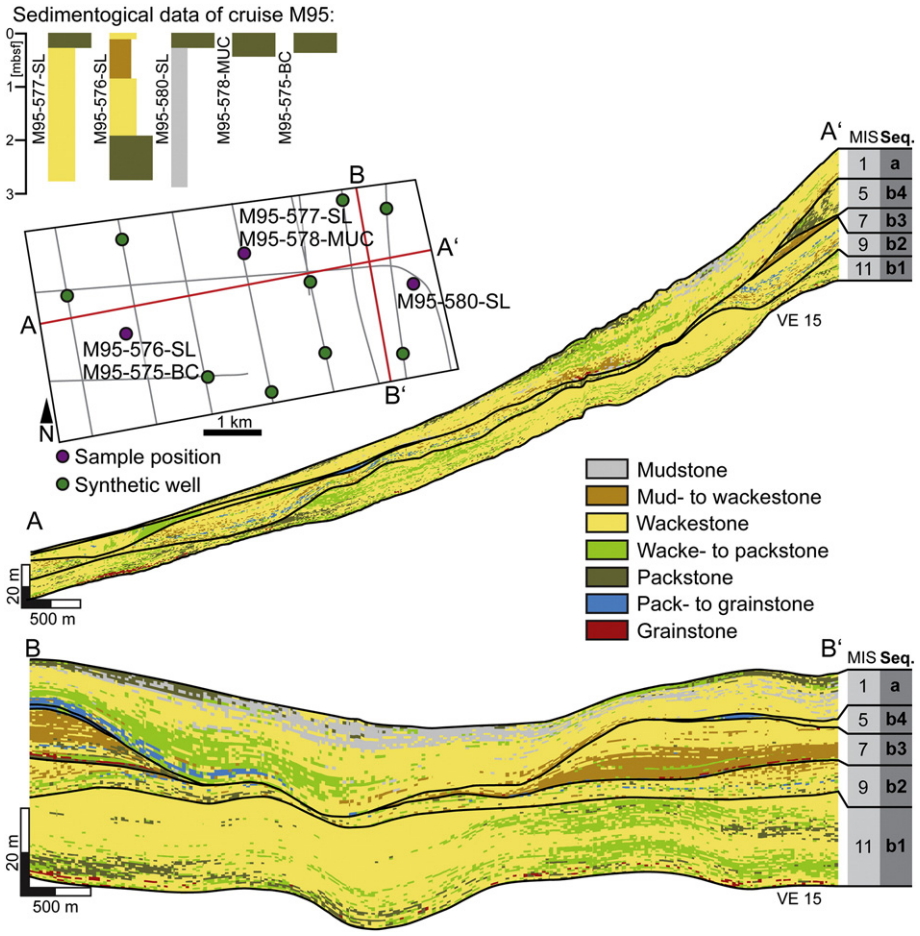

Fig. 17. Stochastic facies model for the northern study area (see location in Fig. 1C). The model shows the facies heterogeneities along-slope and across strike of the slope within the succession of the sequences b1–b4 and a. MIS = Marine Isotope Stage.

Ginsburg, 1981; Playton et al., 2010), where the slopes are fed by line sources, the sediment coarsens with increasing distance from the platform margin, and lateral facies changes are caused by differences in source-sediment grain sizes and textures. Facies heterogeneities along the strike of a carbonate slope make the development depositional models challenging. An improved understanding of such facies heterogeneities is also important in reservoir modeling, because facies alternations at small scales lead to significant changes in the spatial petrophysical properties, such as porosity and permeability (Lucia, 1995).

In the south of the GBB slope, the impact of the currents on the sediment distribution is weak and the exported fine-grained platform sediments such as wackestone form the highstand wedge as part of the periplatform drift. During sea-level lowstands, the coarser-grained sediments form condensed lowstand intervals. This along-slope layer-cake stratigraphy fits well into simplified reservoir models, which predict the same facies and petrophysical properties at the same stratigraphic level (Borgomano et al., 2008; Alnazghah et al., 2013).

In the northern part of the slope, where the current impact is strong, formation and filling of large depressions induces facies heterogeneities at an interwell-scale (Fig. 17). During sea-level lowering, extensive erosion formed isolated sedimentary bodies of the same facies, bounded by unconformities and separated by large depressions (Fig. 17). Platform-derived sediments fill these depressions, during the subsequent sea-level rise and highstand (Fig. 17). This alternation of deposition and erosion forms a complex facies distribution. The infill is not homogenous and coarsens towards the flanks as the result of sea-floor winnowing by bottom currents (Betzler et al., 2014). The encountered facies heterogeneities are beyond the resolution of reflection seismic data and make a reservoir characterization complicated.

5.3. The role of contour currents on the slope sedimentation along the leeward slope

Various authors have recognized an influence of the currents on the leeward slope of GBB (Schlager and Ginsburg, 1981; Ball et al., 1987; Anselmetti et al., 2000; Rendle and Reijmer, 2002; Rendle-Bühring and Reijmer, 2005; Bergman, 2005; Betzler et al., 2014; Wunsch et al., 2016; Principaud et al., 2016). The herein presented data document an increasing influence of the current regime on the sedimentation and the slope architecture towards the north of the study area. In the southern part, where only the north-directed currents acts on the slope, the current influence is low and restricted to the toe of slope. At the toe of slope, the contour current winnows the sediments and probably prevents the leeward slope from further westward progradation. Towards the north, the current impact gradually increases with the coalescence of north-directed contour currents and the Florida current. Current winnowing and drift migration formed a large moat. Continuous winnowing triggered the incision of channels and the accumulation of large mass transport complexes. In this context, it can be speculated if continuous winnowing also favors the large slope failures that occurred during the middle and upper Pleistocene (sequences b1 to b4).

The current control on the slope must be even higher north of the study area, where the Florida Current bends towards the north along the slope of GBB (Fig. 1A). The present position and shape of this slope segment reveal the role of the currents in inhibiting slope progradation

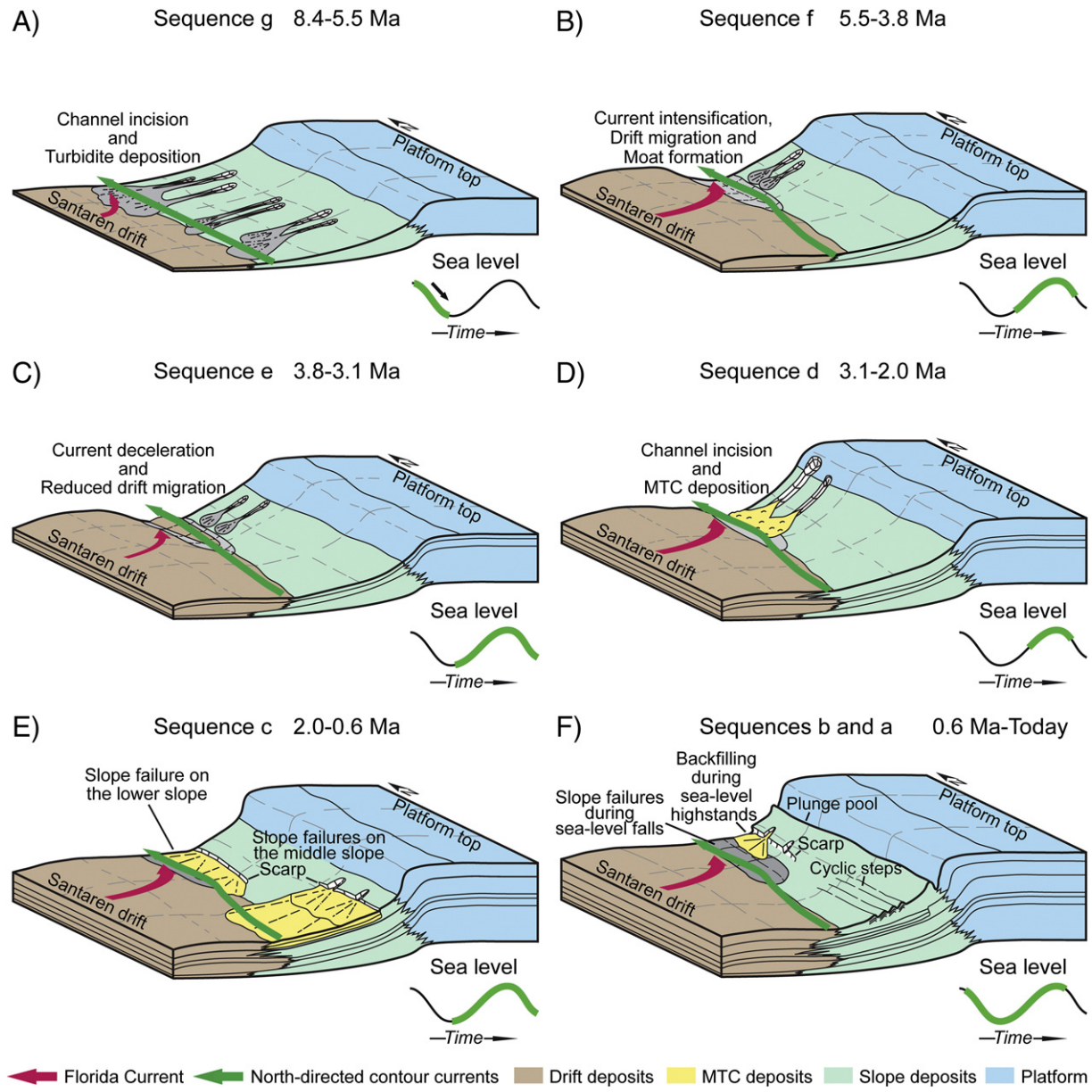

Fig. 18. Depositional model form the evolution of the leeward slope of Great Bahama Bank, see discussion for details. Arrows indicate the current directions.

(Ball et al., 1987). Large parts of the lower slope are winnowed and show no Holocene sediment cover (Principaud, 2015). In this area, the basinal drift sedimentation was initiated during the Miocene and evolved throughout successive phases of growth and lateral migration (Principaud et al., 2016). During the Late Pliocene and Pleistocene, large slope failures displaced slope material as mass-transport complexes into the basin (Principaud et al., 2015, 2016). These large slope failures occurred simultaneously with the accumulation of MTC deposits along the toe of slope, described in this study. Regarding the higher current impact on the slope, oversteepening of the toe of slope by current winnowing is therefore proposed as a potential trigger mechanism for slope failures along this part of the leeward slope.

6. Conclusions

A simple model of sea-level control on the sedimentary dynamics of carbonate platform slopes cannot explain all features of carbonate platform slope geometry. The herein presented data indicate that contour currents are an underestimated factor that induce re-sedimentation processes and shape the slope geometry. Along the leeward slope of GBB, current impact increases from south to north and is highest where the contour currents coalesce with the Florida Currents. In this slope segment, constant current winnowing oversteepens the toe of slope triggering slope failures, incision of channels, and probably the accumulation of large mass transport complexes. To the south, large slope failures were rare and occurred primarily during sea level lowering. Under such circumstances, large channels incise along the complete leeward slope of GBB (e.g. sequence g). Rather than the simple occurrence of a sea-level drop, changes in the cyclicity or the amplitude of sea-level fluctuations seem to be important factors in triggering slope failures. Large slope failures occurred during the MPT and the MBE; periods characterized by sea-level fluctuations of varying amplitudes. The differences between the northern and southern part of the study area are also reflected in the facies distribution along the slope. In the north, where the current impact is strong, the facies distribution is complex. Facies distribution varies in both, the downslope and the along-strike

direction. In the southern part of the study area, where the current influence is weak, the facies heterogeneities occur primarily in downslope direction.

Acknowledgments

We thank the officers and the crew of the R/V Meteor cruise M95 CICARB for efficient assistance. We thank the entire Scientific Shipboard Party of Cruise M95 CICARB for their help in collecting the geophysical and sedimentologic data. A special thanks goes to Juliane Ludwig, Ilona Schutter and Freimut von Borstel for their incredible work and efforts during the cruise. Linda Schiebel analyzed many sedimentological samples from the cruise that are incorporated in this manuscript. Deniz Kula, who had a grant from the Turkish government, helped in processing the data. G.P. Eberli received financial support from the industrial associates to the CSL — Center for Carbonate Research at the University of Miami. J.J.G. Reijmer received support from the Carbonate Sedimentology Group at the Vrije Universiteit Amsterdam, The Netherlands. We thank Schlumberger for providing the Petrel E&P software platform. The German Research Foundation (DFG) is gratefully acknowledged for financial support. The position of Marco Wunsch was funded within the cluster of Excellence "Integrated Climate System Analysis and Prediction" (CliSAP) at University of Hamburg. We thank the Editor in Chief Brian Jones and the reviewer Ángel Puga Bernabéu and Erwin Adams for their careful reviews.

References

Alnazghah, M.H., Bádenas, B., Pomar, L., Aurell, M., Morsilli, M., 2013. Facies heterogeneity at interwell-scale in a carbonate ramp, Upper Jurassic, NE Spain. Marine and Petroleum Geology 44:140–163. https://doi.org/10.1016/j.marpetgeo.2013.03.004.

Anselmetti, F.S., Eberli, G.P., Ding, Z.-D., 2000. From the Great Bahama Bank into the Straits of Florida: a margin architecture controlled by sea-level fluctuations and ocean currents. Geological Society of America Bulletin 112:829–844. https://doi.org/10.1130/0016-7606(2000)112<829:FTGBBI>2.0.CO;2.

Ball, M.M., Dillon, W.P., Wilber, R.J., 1987. Comment and reply on "Segmentation and coalescence of Cenozoic carbonate platforms, northwestern Great Bahama Bank". Geology 15:1081–1082. https://doi.org/10.1130/0091-7613(1987)15<1081:CAROSA>2.0.CO;2.

Berger, W.H., Wefer, G., 2003. On the dynamics of the ice ages: Stage-11 Paradox, Mid-Brunhes climate shift, and 100-ky cycle. In: Droxler, A.W., Poore, R.Z., Burckle, L.H. (Eds.), Geophysical Monograph Series. American Geophysical Union, Washington D. C.:pp. 41–59 https://doi.org/10.1029/137GM04.

Bergman, K.L., 2005. Seismic Analysis of Paleocurrent Features in the Florida Straits: Insights into the Paleo-Florida Current, Upstream Tectonics, and the Atlantic–Caribbean Connection. University of Miami.

Bergman, K.L., Westphal, H., Janson, X., Poiriez, A., Eberli, G.P., 2010. Controlling parameters on facies geometries of the Bahamas, an isolated carbonate platform environment. In: Westphal, H., Riegl, B., Eberli, G.P. (Eds.), Carbonate Depositional Systems: Assessing Dimensions and Controlling Parameters. Springer Netherlands, Dordrecht, The Netherlands, pp. 5–80.

Bernet, K., Eberli, G.P., Gilli, A., 2000. Turbidite frequency and composition in the distal part of the Bahamas Transect. In: Swart, P.K., Eberli, G.P., Malone, M.J., Sarg, J.F. (Eds.), Proceedings of the Ocean Drilling Program, 166 Scientific Results. Ocean Drilling Program, College Station, TX, USA, pp. 45–60.

Betzler, C., Reijmer, J.J.G., Bernet, K., Eberli, G.P., Anselmetti, F.S., 1999. Sedimentary patterns and geometries of the Bahamian outer carbonate ramp (Miocene-Lower Pliocene, Great Bahama Bank). Sedimentology 46:1127–1143. https://doi.org/10.1046/j.1365-3091.1999.00268.x.

Betzler, C., Lindhorst, S., Eberli, G.P., Lüdmann, T., Möbius, J., Ludwig, J., Schutter, I., Wunsch, M., Reijmer, J.J.G., Hübscher, C., 2014. Periplatform drift: the combined result of contour current and off-bank transport along carbonate platforms. Geology 42: 871–874. https://doi.org/10.1130/G35900.1.

Billups, K., 2002. Late Miocene through early Pliocene deep water circulation and climate change viewed from the sub-Antarctic South Atlantic. Palaeogeography, Palaeoclimatology, Palaeoecology 185:287–307. https://doi.org/10.1016/S0031-0182(02)00340-1.

Borgomano, J.R.F., Fournier, F., Viseur, S., Rijkels, L., 2008. Stratigraphic well correlations for 3-D static modeling of carbonate reservoirs. AAPG Bulletin 92: 789–824. https://doi.org/10.1306/02210807078.

Chabaud, L., Ducassou, E., Tournadour, E., Mulder, T., Reijmer, J.J.G., Conesa, G., Giraudeau, J., Hanquiez, V., Borgomano, J., Ross, L., 2016. Sedimentary processes determining the modern carbonate periplatform drift of Little Bahama Bank. Marine Geology 378: 213–229. https://doi.org/10.1016/j.margeo.2015.11.006.

Clark, P.U., Archer, D., Pollard, D., Blum, J.D., Rial, J.A., Brovkin, V., Mix, A.C., Pisias, N.G., Roy, M., 2006. The middle Pleistocene transition: characteristics, mechanisms, and implications for long-term changes in atmospheric pCO_2. Quaternary Science Reviews 25: 3150–3184. https://doi.org/10.1016/j.quascirev.2006.07.008.

Deutsch, C.V., Journel, A.G., 1998. GSLIB: Geostatistical Software Library and User's Guide. 2nd editon. Oxford University Press, New York, USA.

Droxler, A.W., Schlager, W., 1985. Glacial versus interglacial sedimentation rates and turbidite frequency in the Bahamas. Geology 13:799–802. https://doi.org/10.1130/0091-7613(1985)13<799:GVISRA>2.0.CO;2.

Droxler, A.W., Schlager, W., Whallon, C.C., 1983. Quaternary aragonite cycles and oxygen-isotope record in Bahamian carbonate ooze. Geology 11:235–239. https://doi.org/10.1130/0091-7613(1983)11<235:QACAOR>2.0.CO;2.

Dunham, R.J., 1962. Classification of carbonate rocks according to depositional textures. In: Ham, W.E. (Ed.), Classification of Carbonate Rocks—A Symposium. AAPG Memoir. American Association of Petroleum Geologists, Tulsa, OK, USA, pp. 108–121.

Eberli, G.P., 1991. Growth and demise of isolated carbonate platforms: Bahamian controversies. In: Müller, D.W., MacKenzie, J.A., Weissert, H. (Eds.), Controversies in Modern Geology. Acad. Press, London, United Kingdom, pp. 205–232.

Eberli, G.P., 2000. The record of Neogene sea-level changes in the prograding carbonates along the Bahamas Transect—Leg 166 synthesis. In: Swart, P.K., Eberli, G.P., Malone, M.J., Sarg, J.F. (Eds.), Proceedings of the Ocean Drilling Program, 166 Scientific Results. Proceedings of the Ocean Drilling Program. Ocean Drilling Program, College Station, TX, USA, pp. 167–177.

Eberli, G.P., Ginsburg, R.N., 1987. Segmentation and coalescence of Cenozoic carbonate platforms, northwestern Great Bahama Bank. Geology 15:75–79. https://doi.org/10.1130/0091-7613(1987)15<75:SACOCC>2.0.CO;2.

Eberli, G.P., Swart, P.K., Malone, M.J., Shipboard Scientific Party (Eds.), 1997. Proceedings of the Ocean Drilling Program, 166 Initial Reports. Proceedings of the Ocean Drilling Program. Ocean Drilling Program, College Station, TX, USA.

Eberli, G.P., Anselmetti, F.S., Kroon, D., Sato, T., Wright, J.D., 2002. The chronostratigraphic significance of seismic reflections along the Bahamas Transect. Marine Geology 185: 1–17. https://doi.org/10.1016/S0025-3227(01)00287-0.

Eberli, G.P., Anselmetti, F.S., Betzler, C., Van Konijnenburg, J.-H., Bernoulli, D., 2004. Carbonate platform to basin transitions on seismic data and in outcrops: Great Bahama Bank and the Maiella Platform Margin, Italy. In: Eberli, G.P., Masaferro, J.L., Sarg, J.F. (Eds.), Seismic Imaging of Carbonate Reservoirs and Systems. American Association of Petroleum Geologists, Tulsa, OK, USA, pp. 207–250.

Embry, A.F., Klovan, J.E., 1971. A late Devonian reef tract on northeastern Banks Island, N.W.T. Bulletin of Canadian Petroleum Geology 19, 730–781.

EPICA Community, 2004. Eight glacial cycles from an Antarctic ice core. Nature 429: 623–628. https://doi.org/10.1038/nature02599.

Gradstein, F.M., Ogg, J.G., Schmitz, M.D., Ogg, G.M. (Eds.), 2012. The Geologic Time Scale 2012, 1st ed. Elsevier, Kidlington, UK.

Grammer, G.M., Ginsburg, R.N., Harris, P.M., 1993. Timing of deposition, diagenesis, and failure of steep carbonate slopes in response to a high-amplitude/high-frequency fluctuation in sea level, Tongue of the Ocean, Bahamas. In: Loucks, R.G., Sarg, J.F., American Association of Petroleum Geologists (Eds.), Carbonate Sequence Stratigraphy: Recent Developments and Applications. American Association of Petroleum Geologists, Tulsa, OK, USA, pp. 107–131.

Grasmueck, M., Eberli, G.P., Viggiano, D.A., Correa, T., Rathwell, G., Luo, J., 2006. Autonomous underwater vehicle (AUV) mapping reveals coral mound distribution, morphology, and oceanography in deep water of the Straits of Florida. Geophysical Research Letters 33. https://doi.org/10.1029/2006GL027734.

Haug, G.H., Tiedemann, R., 1998. Effect of the formation of the Isthmus of Panama on Atlantic Ocean thermohaline circulation. Nature 393:673–676. https://doi.org/10.1038/31447.

Haug, G.H., Tiedemann, R., Zahn, R., Ravelo, A.C., 2001. Role of Panama uplift on oceanic freshwater balance. Geology 29:207–210. https://doi.org/10.1130/0091-7613(2001)029<0207:ROPUOO>2.0.CO;2.

Hearty, P.J., 1998. The geology of Eleuthera Island, Bahamas: a Rosetta Stone of Quaternary stratigraphy and sea-level history. Quaternary Science Reviews 17: 333–355. https://doi.org/10.1016/S0277-3791(98)00046-8.

Hearty, P.J., Neumann, A.C., 2001. Rapid sea level and climate change at the close of the Last Interglaciation (MIS 5e): evidence from the Bahama Islands. Quaternary Science Reviews 20:1881–1895. https://doi.org/10.1016/S0277-3791(01)00021-X.

Hearty, P.J., Hollin, J.T., Neumann, A.C., O'Leary, M.J., McCulloch, M., 2007. Global sea-level fluctuations during the Last Interglaciation (MIS 5e). Quaternary Science Reviews 26: 2090–2112. https://doi.org/10.1016/j.quascirev.2007.06.019.

Henderson, G.M., Robinson, L.F., Cox, K., Thomas, A.L., 2006. Recognition of non-Milankovitch sea-level highstands at 185 and 343 thousand years ago from U–Th dating of Bahamas sediment. Quaternary Science Reviews 25:3346–3358. https://doi.org/10.1016/j.quascirev.2006.03.003.

Hine, A.C., Steinmetz, J.C., 1984. Cay Sal Bank, Bahamas — a partially drowned carbonate platform. Marine Geology 59:135–164. https://doi.org/10.1016/0025-3227(84)90091-4.

Hine, A.C., Wilber, R.J., Neumann, A.C., 1981. Carbonate sand bodies along contrasting shallow bank margins facing open seaways in northern Bahamas. AAPG Bulletin 65, 261–290.

Jaime Gómez-Hernández, J., Mohan Srivastava, R., 1990. ISIM3D: an ANSI-C three-dimensional multiple indicator conditional simulation program. Computers & Geosciences 16:395–440. https://doi.org/10.1016/0098-3004(90)90010-Q.

Jo, A., Eberli, G.P., Grasmueck, M., 2015. Margin collapse and slope failure along southwestern Great Bahama Bank. Sedimentary Geology 317:43–52. https://doi.org/10.1016/j.sedgeo.2014.09.004.

Journel, A.G., 1983. Nonparametric estimation of spatial distributions. Journal of the International Association for Mathematical Geology 15:445–468. https://doi.org/10.1007/BF01031292.

Kaneps, A.G., 1979. Gulf stream: velocity fluctuations during the Late Cenozoic. Science 204:297–301. https://doi.org/10.1126/science.204.4390.297.

Kendall, C.G.S.C., Schlager, W., 1981. Carbonates and relative changes in sea level. Marine Geology 44, 181–212.

Kenter, J.A.M., 1990. Carbonate platform flanks: slope angle and sediment fabric. Sedimentology 37:777–794. https://doi.org/10.1111/j.1365-3091.1990.tb01825.x.
Kenter, J.A.M., Ginsburg, R.N., Troelstra, S.R., 2001. Sea-level-driven sedimentation patterns on the slope and margin. In: Ginsburg, R.N., Warzeski, E.R. (Eds.), Subsurface Geology of a Prograding Carbonate Platform Margin, Great Bahama Bank: Results of the Bahamas Drilling Project. SEPM Special Publication. SEPM (Society for Sedimentary Geology), Tulsa, OK, USA, pp. 61–100.
Kievman, C.M., 1998. Match between late Pleistocene Great Bahama Bank and deep-sea oxygen isotope records of sea level. Geology 26:635–638. https://doi.org/10.1130/0091-7613(1998)026<0635:MBLPGB>2.3.CO;2.
Kourafalou, V.H., Kang, H., 2012. Florida Current meandering and evolution of cyclonic eddies along the Florida Keys Reef Tract: are they interconnected? Journal of Geophysical Research 117. https://doi.org/10.1029/2011JC007383.
Kroon, D., Reijmer, J.J.G., Rendle, R.H., 2000. Mid- to late-Quaternary variations in the oxygen isotope signature of *Globigerinoides ruber* at Site 1006 in the western subtropical Atlantic. In: Swart, P.K., Eberli, G.P., Malone, M.J., Sarg, J.F. (Eds.), Proceedings of the Ocean Drilling Program. 166 Scientific Results. Ocean Drilling Program, College Station, TX, USA, pp. 13–22.
Ladd, J.W., Sheridan, R.E., 1987. Seismic stratigraphy of the Bahamas. American Association of Petroleum Geologists Bulletin 71, 719–736.
Leaman, K.D., Vertes, P.S., Atkinson, L.P., Lee, T.N., Hamilton, P., Waddell, E., 1995. Transport, potential vorticity, and current/temperature structure across Northwest Providence and Santaren Channels and the Florida Current off Cay Sal Bank. Journal of Geophysical Research 100:8561–8569. https://doi.org/10.1029/94JC01436.
Lee, T.N., Leaman, K., Williams, E., Berger, T., Atkinson, L., 1995. Florida Current meanders and gyre formation in the southern Straits of Florida. Journal of Geophysical Research 100:8607–8620. https://doi.org/10.1029/94JC02795.
Lucia, F.J., 1995. Rock-fabric/petrophysical classification of carbonate pore space for reservoir characterization. AAPG Bulletin 79:1275–1300. https://doi.org/10.1306/7834D4A4-1721-11D7-8645000102C1865D.
Lüdmann, T., Paulat, M., Betzler, C., Möbius, J., Lindhorst, S., Wunsch, M., Eberli, G.P., 2016. Carbonate mounds in the Santaren Channel, Bahamas: a current-dominated periplatform depositional regime. Marine Geology 376:69–85. https://doi.org/10.1016/j.margeo.2016.03.013.
Malone, M.J., 2000. Data report: geochemistry and mineralogy of periplatform carbonate sediments: sites 1006, 1008, and 1009. In: Swart, P.K., Eberli, G.P., Malone, M.J., Sarg, J.F. (Eds.), Proceedings of the Ocean Drilling Program, 166 Scientific Results. Ocean Drilling Program, College Station, TX, USA, pp. 145–152.
Malone, M.J., Slowey, N.C., Henderson, G.M., 2001. Early diagenesis of shallow-water periplatform carbonate sediments, leeward margin, Great Bahama Bank (Ocean Drilling Program Leg 166). Geological Society of America Bulletin 113:881–894. https://doi.org/10.1130/0016-7606(2001)113<0881:EDOSWP>2.0.CO;2.
Manfrino, C., Ginsburg, R.N., 2001. Pliocene to Pleistocene depositional history of the Upper Platform Margin. In: Ginsburg, R.N., Warzeski, E.R. (Eds.), Subsurface Geology of a Prograding Carbonate Platform Margin, Great Bahama Bank: Results of the Bahamas Drilling Project. SEPM Special Publication. SEPM (Society for Sedimentary Geology), Tulsa, OK, USA, pp. 61–100.
Masaferro, J.L., Eberli, G.P., 1999. Jurassic–Cenozoic structural evolution of the southern Great Bahama Bank. In: Mann, P. (Ed.), Sedimentary Basins of the World. Elsevier, Amsterdam, The Netherlands, pp. 167–193.
Maslin, M.A., Brierley, C.M., 2015. The role of orbital forcing in the Early Middle Pleistocene Transition. Quaternary International 389:47–55. https://doi.org/10.1016/j.quaint.2015.01.047.
Mulder, T., Ducassou, E., Eberli, G.P., Hanquiez, V., Gonthier, E., Kindler, P., Principaud, M., Fournier, F., Leonide, P., Billeaud, I., Marsset, B., Reijmer, J.J.G., Bondu, C., Joussiaume, R., Pakiades, M., 2012. New insights into the morphology and sedimentary processes along the western slope of Great Bahama Bank. Geology 40:603–606. https://doi.org/10.1130/G32972.1.
Mullins, H.T., Lynts, G.W., 1977. Origin of the northwestern Bahama platform: review and reinterpretation. Geological Society of America Bulletin 88:1447–1461. https://doi.org/10.1130/0016-7606(1977)88<1447:OOTNBP>2.0.CO;2.
Mullins, H.T., Heath, K.C., Mark van Buren, H., Newton, C.R., 1984. Anatomy of a modern open-ocean carbonate slope: northern Little Bahama Bank. Sedimentology 31:141–168. https://doi.org/10.1111/j.1365-3091.1984.tb01956.x.
Neumann, A.C., Ball, M.M., 1970. Submersible observations in the Straits of Florida: geology and bottom currents. Geological Society of America Bulletin 81:2861–2873. https://doi.org/10.1130/0016-7606(1970)81[2861:SOITSO]2.0.CO;2.
Neumann, A.C., Hearty, P.J., 1996. Rapid sea-level changes at the close of the last interglacial (substage 5e) recorded in Bahamian island geology. Geology 24:775–778. https://doi.org/10.1130/0091-7613(1996)024<0775:RSLCAT>2.3.CO;2.
Pisias, N.G., Moore, T.C., 1981. The evolution of Pleistocene climate: a time series approach. Earth and Planetary Science Letters 52:450–458. https://doi.org/10.1016/0012-821X(81)90197-7.
Playton, T.E., Janson, X., Kerans, C., 2010. Carbonate slopes. In: James, N.P., Dalrymple, R.W. (Eds.), Facies Models 4. Geolog. Assoc. of Canada, St. Johns, pp. 449–476.
Principaud, M., 2015. Morphologie, Architecture et dynamique Sédimentaire d'une pente carbonatée moderne: le Great Bahama Bank (Bahamas). (Published PhD thesis). University of Bordeaux, Bordeaux.
Principaud, M., Mulder, T., Gillet, H., Borgomano, J., 2015. Large-scale carbonate submarine mass-wasting along the northwestern slope of the Great Bahama Bank (Bahamas): morphology, architecture, and mechanisms. Sedimentary Geology 317:27–42. https://doi.org/10.1016/j.sedgeo.2014.10.008.
Principaud, M., Ponte, J.-P., Mulder, T., Gillet, H., Robin, C., Borgomano, J., 2016. Slope-to-basin stratigraphic evolution of the carbonate northwestern Great Bahama Bank (Bahamas) during the Neogene to Quaternary: interactions between downslope and bottom currents deposits. Basin Research https://doi.org/10.1111/bre.12195.
Raymo, M.E., Hodell, D., Jansen, E., 1992. Response of deep ocean circulation to initiation of northern hemisphere glaciation (3–2 MA). Paleoceanography 7:645–672. https://doi.org/10.1029/92PA01609.
Raymo, M.E., Grant, B., Horowitz, M., Rau, G.H., 1996. Mid-Pliocene warmth: stronger greenhouse and stronger conveyor. Marine Micropaleontology 27:313–326. https://doi.org/10.1016/0377-8398(95)00048-8.
Reijmer, J.J.G., Schlager, W., Droxler, A.W., 1988. Pliocene–Pleistocene sedimentation cycles in a Bahamian basin. In: Austin Jr., J.A., Schlager, W., et al. (Eds.), Proceedings of the Ocean Drilling Program, 101 Scientific Results. Proceedings of the Ocean Drilling Program. Ocean Drilling Program, College Station, TX, USA:pp. 213–220. https://doi.org/10.2973/odp.proc.sr.101.1988.
Reijmer, J.J., Betzler, C., Kroon, D., Tiedemann, R., Eberli, G.P., 2002. Bahamian carbonate platform development in response to sea-level changes and the closure of the Isthmus of Panama. International Journal of Earth Sciences 91:482–489. https://doi.org/10.1007/s00531-001-0235-x.
Rendle, R.H., Reijmer, J.J.G., 2002. Quaternary slope development of the western, leeward margin of the Great Bahama Bank. Marine Geology 185:143–164. https://doi.org/10.1016/S0025-3227(01)00294-8.
Rendle, R.H., Reijmer, J.J.G., Kroon, D., Henderson, G.M., 2000. Mineralogy and sedimentology of the Pleistocene to Holocene on the leeward margin of Great Bahama Bank. In: Eberli, G.P., Swart, P.K., Malone, M.J., et al. (Eds.), Proceedings of the Ocean Drilling Program. Scientific Results Leg 166. Ocean Drilling Program, College Station, TX, USA, pp. 61–76.
Rendle-Bühring, R.H., Reijmer, J.J.G., 2005. Controls on grain-size patterns in periplatform carbonates: marginal setting versus glacio-eustacy. Sedimentary Geology 175:99–113. https://doi.org/10.1016/j.sedgeo.2004.12.025.
Robinson, L.F., Henderson, G.M., Slowey, N.C., 2002. U–Th dating of marine isotope stage 7 in Bahamas slope sediments. Earth and Planetary Science Letters 196:175–187. https://doi.org/10.1016/S0012-821X(01)00610-0.
Roth, S., Reijmer, J.J.G., 2004. Holocene Atlantic climate variations deduced from carbonate periplatform sediments (leeward margin, Great Bahama Bank). Paleoceanography 19(1):PA1003. https://doi.org/10.1029/2003PA000885.
Roth, S., Reijmer, J.J.G., 2005. Holocene millennial to centennial carbonate cyclicity recorded in slope sediments of the Great Bahama Bank and its climatic implications. Sedimentology 52:161–181. https://doi.org/10.1111/j.1365-3091.2004.00684.x.
Schlager, W., Camber, O., 1986. Submarine slope angles, drowning unconformities, and self-erosion of limestone escarpments. Geology 14:762–765. https://doi.org/10.1130/0091-7613(1986)14<762:SSADUA>2.0.CO;2.
Schlager, W., Ginsburg, R.N., 1981. Bahama carbonate platforms — the deep and the past. Marine Geology 44:1–24. https://doi.org/10.1016/0025-3227(81)90111-0.
Schlager, W., Reijmer, J.J.G., Droxler, A.W., 1994. Highstand shedding of carbonate platforms. SEPM Journal of Sedimentary Research B64:270–281. https://doi.org/10.1306/D4267FAA-2B26-11D7-8648000102C1865D.
Schmitz, W.J., Richardson, P.L., 1991. On the sources of the Florida Current. Deep Sea Research Part A. Oceanographic Research Papers 38:379–409. https://doi.org/10.1016/S0198-0149(12)80018-5.
Schnyder, J.S.D., Eberli, G.P., Kirby, J.T., Shi, F., Tehranirad, B., Mulder, T., Ducassou, E., Hebbeln, D., Wintersteller, P., 2016. Tsunamis caused by submarine slope failures along western Great Bahama Bank. Scientific Reports 6. https://doi.org/10.1038/srep35925.
Shackleton, N.J., Opdyke, N.D., 1976. Oxygen-isotope and paleomagnetic stratigraphy of Pacific Core V28-239 Late Pliocene to Latest Pleistocene. In: Cune, R.M., Hays, J.D. (Eds.), Investigation of Late Quaternary Paleoceanography and Paleoclimatology. Geological Society of America Memoir. Geological Society of America, Boulder, CO, USA, pp. 449–463.
Steph, S., Tiedemann, R., Prange, M., Groeneveld, J., Nürnberg, D., Reuning, L., Schulz, M., Haug, G.H., 2006. Changes in Caribbean surface hydrography during the Pliocene shoaling of the Central American Seaway. Paleoceanography 21. https://doi.org/10.1029/2004PA001092.
Steph, S., Tiedemann, R., Prange, M., Groeneveld, J., Schulz, M., Timmermann, A., Nürnberg, D., Rühlemann, C., Saukel, C., Haug, G.H., 2010. Early Pliocene increase in thermohaline overturning: a precondition for the development of the modern equatorial Pacific cold tongue. Paleoceanography 25. https://doi.org/10.1029/2008PA001645.
Tinker, S.W., 1998. Shelf-to-basin facies distributions and sequence stratigraphy of a steep-rimmed carbonate margin; Capitan depositional system, McKittrick Canyon, New Mexico and Texas. Journal of Sedimentary Research 68:1146–1174. https://doi.org/10.2110/jsr.68.1146.
Tournadour, E., Mulder, T., Borgomano, J., Hanquiez, V., Ducassou, E., Gillet, H., 2015. Origin and architecture of a Mass Transport Complex on the northwest slope of Little Bahama Bank (Bahamas): relations between off-bank transport, bottom current sedimentation and submarine landslides. Sedimentary Geology 317:9–26. https://doi.org/10.1016/j.sedgeo.2014.10.003.
Verwer, K., Merino-Tome, O., Kenter, J.A.M., Della Porta, G., 2009. Evolution of a high-relief carbonate platform slope using 3D digital outcrop models: Lower Jurassic Djebel Bou Dahar, High Atlas, Morocco. Journal of Sedimentary Research 79:416–439. https://doi.org/10.2110/jsr.2009.045.
Wang, J., Mooers, C.N.K., 1997. Three-dimensional perspectives of the Florida current: transport, potential vorticity, and related dynamical properties. Dynamics of Atmospheres and Oceans 27:135–149. https://doi.org/10.1016/S0377-0265(97)00004-3.
Wilber, R.J., Milliman, J.D., Halley, R.B., 1990. Accumulation of bank-top sediment on the western slope of Great Bahama Bank: rapid progradation of a carbonate megabank. Geology 18:970–974. https://doi.org/10.1130/0091-7613(1990)018<0970:AOBTSO>2.3.CO;2.
Wilber, R.J., Whitehead, J., Halley, R.B., Milliman, J.D., Wilson, P.A., Roberts, H.H., 1993. Carbonate-periplatforrn sedimentation by density flows: a mechanism for rapid off-

bank and vertical transport of shallow-water fines: comment and reply. Geology 21: 667–668. https://doi.org/10.1130/0091-7613(1993)021<0667:CPSBDF>2.3.CO;2.

Wilson, P.A., Roberts, H.H., 1992. Carbonate-periplatform sedimentation by density flows: a mechanism for rapid off-bank and vertical transport of shallow-water fines. Geology 20:713–716. https://doi.org/10.1130/0091-7613(1992)020<0713:CPSBDF>2.3.CO;2.

Wilson, P.A., Roberts, H.H., 1995. Density cascading: off-shelf sediment transport, evidence and implications, Bahama Banks. Journal of Sedimentary Research 65A: 45–56. https://doi.org/10.1306/D426801D-2B26-11D7-8648000102C1865D.

Wright, J.D., Kroon, D., 2000. Planktonic foraminiferal biostratigraphy of leg 166. In: Swart, P.K., Eberli, G.P., Malone, M.J., Sarg, J.F. (Eds.), Proceedings of the Ocean Drilling Program, 166 Scientific Results. Ocean Drilling Program, College Station, TX, USA, pp. 3–12.

Wunsch, M., Betzler, C., Lindhorst, S., Lüdmann, T., Eberli, G.P., 2016. Sedimentary dynamics along carbonate slopes (Bahamas archipelago). Sedimentology 64: 631–657. https://doi.org/10.1111/sed.12317.